Project Report
TIP-103

Using Sparse Sensors to Locate Signals in the Presence of Interference: FY19 RF Systems Technical Investment Program

S. Appadwedula
K.W. Forsythe
N. Yazdani

3 January 2020

Lincoln Laboratory
MASSACHUSETTS INSTITUTE OF TECHNOLOGY
LEXINGTON, MASSACHUSETTS

This material is based upon work supported by the Under Secretary of Defense for Research and Engineering and United States Air Force under Air Force Contract No. FA8702-15-D-0001.

This report is the result of studies performed at Lincoln Laboratory, a federally funded research and development center operated by Massachusetts Institute of Technology. This material is based upon work supported by the Under Secretary of Defense for Research and Engineering and United States Air Force under Air Force Contract No. FA8702-15-D-0001. Any opinions, findings, conclusions or recommendations expressed in this material are those of the author(s) and do not necessarily reflect the views of the Under Secretary of Defense for Research and Engineering and United States Air Force.

Massachusetts Institute of Technology
Lincoln Laboratory

Using Sparse Sensors to Locate Signals in the Presence of Interference: FY19 RF Systems Technical Investment Program

S. Appadwedula
K.W. Forsythe
Group 62

N. Yazdani
Group 64

Project Report TIP-103

3 January 2020

Lexington Massachusetts

This page intentionally left blank.

ABSTRACT

Geolocation of communications signals is an important capability in many civilian, commercial, and defense applications. In many scenarios, the communications signals of interest are wideband and observed in the presence of background interference. Adaptive processing on multiple sensors can cancel background interference and obtain copy and parameter estimates of the signal of interest. Current wideband approaches for localization with multiple sensors primarily use cross correlation, which is relevant when the signal of interest and interference are of similar powers. In this report, several new localization approaches are developed to be able to operate in disparate power regimes through the use of adaptive cancellation. The approaches described efficiently handle delay spread through the use of frequency channelization. A particular iterative demodulation approach also handles Doppler spread due to relative sensor movement.

This page intentionally left blank.

ACKNOWLEDGMENTS

This effort was funded by the Radio Frequency (RF) Line program, and the authors would like to thank Gary Hatke and Sean Duffy for their support and technical comments.

Also, the authors would like to thank staff at MIT Lincoln Laboratory for the technical discussions, in particular Cathy Keller and Henry Romero.

This page intentionally left blank.

TABLE OF CONTENTS

TABLE OF CONTENTS
(Continued)

LIST OF FIGURES

LIST OF FIGURES
(Continued)

LIST OF FIGURES

(Continued)

This page intentionally left blank.

1. INTRODUCTION

As low cost sensors and small platforms such as unmanned aerial vehicles (UAVs) are becoming more ubiquitous, there is interest in understanding how using swarms of such platforms can enable or enhance performance in DoD missions. One application of significant interest is signal geolocation. A swarm of small platforms surrounding the signal of interest provides a better detection and geolocation geometry than any single platform based solution can provide, particularly at high altitudes. New signal processing challenges arise with distributed swarm geolocation architectures, and solutions to these challenges are the focus of this report.

Consider the example shown in Figure 1 of a swarm of UAVs, flying over a dense urban area, looking for a particular wideband WiFi or cellular signal. As these frequency bands are reused by many devices, the UAVs see significant co-channel interference, which increases with the sensor coverage region and platform altitude. The spacing and movement of the UAVs creates delay and Doppler frequency shift on the signals at the sensors, requiring complicated signal processing approaches. In this report, several signal processing approaches are developed and analyzed to address these challenges including Adaptive Event Processing (AEP), Multiple Signal Classification (MUSIC), and iterative demodulation.

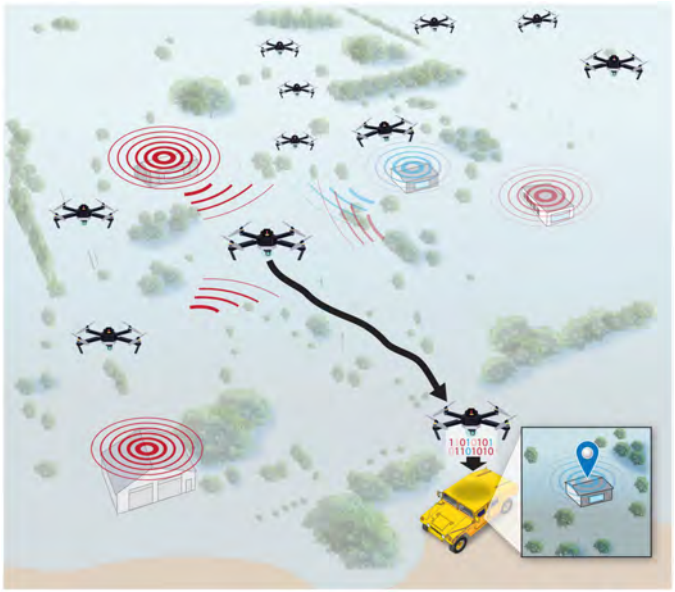

Figure 1. A rescue scenario where UAV sensors are trying to locate signals in the presence of interference. Each UAV in the distributed array collects and stores digital samples before returning to a hub where adaptive beamforming techniques are used to estimate the location of the signals.

The approaches described herein are important not only in enabling wideband geolocation in congested RF environments but also in contested RF environments where receivers are expected to be actively jammed.

The organization of this report is as follows. Section 2 formulates the geolocation problem and covers the simple cases where maximum likelihood (ML) solutions can be derived. Section 3 gives an overview of the multiple signals approaches. Section 4 describes the traditional cross correlation approach and the effect of communications signals sidelobes. Section 5 explains two architectures for dealing with delay spread. Sections 6,7, and 8 describe the beamforming approaches that use the frequency channelization architecture. Section 9 shows the application of the proposed approaches in simulations, and Section 10 concludes the discussion.

2. PROBLEM FORMULATION

The geometry of the geolocation problem covered in this report is described in Figure 2, where K sensors sensors at locations $\mathbf{x}_k, k = 1, \ldots, K$ moving with linear velocity $\dot{\mathbf{x}}_k$ attempt to locate a source at location $\mathbf{x}_0$ that emits a signal $s(t)$. The ability to estimate source position depends on a variety of factors, including signal duration, relative source powers, sensor geometry, signal overlap in time, and noise level at the sensors. Discussed herein are beamforming techniques for estimating the source position using primarily time difference of arrival (TDOA) techniques. Algorithms and architectures are developed to handle the presence of other signals, termed as interferers. It is assumed that the sensors can be synchronized in time and frequency using accurate clocks, but not necessarily in phase due to each having its own phase locked loop (PLL). The locations and velocity of the sensors are assumed to be known through the use of a positioning system such as Global Positioning System (GPS). The raw sensor measurements are assumed to be available at a central location, as this is key to the beamforming techniques to be discussed. The source is not assumed to be cooperative or coordinated with the sensors; however, techniques for communications signals with known waveforms are presented.

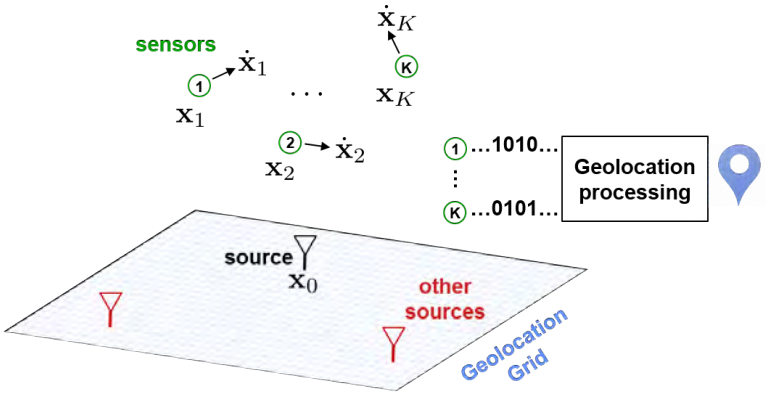

Figure 2. Geometry of the geolocation problem showing a source to be located using possibly moving sensors. Sample data from the sensors is processed at a central location to produce geolocation and waveform estimates of the source.

Consider the continuous-time communications waveform $s(t)$ transmitted at the source as obtained by pulse-modulation of a discrete sequence $b[n]$, e.g. representing BPSK, and frequency-modulated to the carrier frequency f_0

$$s(t) = e^{j2\pi \mathrm{f}_0 t} \sum_{n=0}^{B-1} b[n]\, p(t - nT_c) \tag{1}$$

where $p(t)$ is a band-limited pulse waveform with unit energy, T_c is the pulse spacing in time, and B is the number of pulses.

The discrete-time received waveform at each of the $k = 1, \ldots, K$ sensor platforms, after down-conversion and sampling is

$$z_k[l] = a_k e^{j\phi_k} e^{-j2\pi f_0 \tau_k(t_l)}\, s(t_l - (t_s + \tau_k(t_l))) + \nu_k(t_l) \tag{2}$$

where the receive times are $t_l = l\,T_r$ at samples $l = 0, 1, \ldots, L-1$, t_s is the unknown start time of the source transmission and ν_k is complex white Gaussian noise that is uncorrelated from platform to platform and has the same variance σ^2 (i.e., $\boldsymbol{\nu} \sim \mathcal{CN}(\mathbf{0}, \sigma^2\mathbf{I})$). The terms sensor and platform are used interchangeably throughout this document. The differences in signal-to-noise (SNR) between platforms are captured in a_k, which represents real amplitude scaling. An unknown waveform phase ϕ_k captures transmit phase, down-conversion, antenna and phase due to the receiver.

The time-varying delays from the source to the sensors, $\tau_k(t)$ is described in detail in the next section.

2.1 LINEAR MODEL FOR DELAY

The time-varying delay from user to the platform depends on motion, and results in a transcendental equation due to possible change in the platform position from the time transmission starts at the source to when it arrives at the platform

$$\tau_k(t) = \frac{1}{c}\left\|\mathbf{x}_k(t) - \mathbf{x}_0(t - \tau_k(t))\right\| \tag{3}$$

$$\overset{\text{quasi-static}}{\approx} \frac{1}{c}\left\|\mathbf{x}_k(t) - \mathbf{x}_0(t)\right\| \tag{4}$$

where $\mathbf{x}_k(t)$ is the platform position and $\mathbf{x}_0(t)$ is the source position. Solving for τ is possible as shown in Appendix 1. However, when the source motion is relatively small over a time window of interest, the quasi-static approximation that source position does not depend on the time-varying delay leads to (4). In particular, for linear velocity, the approximation leads to a delay, Doppler interpretation of the time-varying delay.

Consider sensors moving from a starting position $\mathbf{x}_k$ with a fixed velocity vector $\mathbf{v}_k$ over the measurement interval. The source is assumed to be stationary with position $\mathbf{x}_0$ [1]

$$\begin{aligned}
\tau_k(t) &= \frac{1}{c}\left\|\underbrace{\mathbf{x}_k - \mathbf{x}_0}_{\triangleq \boldsymbol{\Delta}\mathbf{x}_0} + \mathbf{v}_k \cdot t\right\| \\
&= \frac{1}{c}\left\|\boldsymbol{\Delta}\mathbf{x}_0\right\| \sqrt{1 + 2\mathbf{v}_k^T \frac{\boldsymbol{\Delta}\mathbf{x}_0}{\left\|\boldsymbol{\Delta}\mathbf{x}_0\right\|^2} \cdot t + \frac{\left\|\mathbf{v}_k\right\|^2}{\left\|\boldsymbol{\Delta}\mathbf{x}_0\right\|^2} \cdot t^2} \\
&\overset{t<<1}{\approx} \frac{1}{c}\left\|\boldsymbol{\Delta}\mathbf{x}_0\right\| \sqrt{1 + 2\mathbf{v}_k^T \frac{\mathbf{u}_0}{\left\|\boldsymbol{\Delta}\mathbf{x}_0\right\|} \cdot t} \\
&\overset{\sqrt{1+x} \approx \frac{x}{2}+1}{\approx} \underbrace{\frac{1}{c}\left\|\boldsymbol{\Delta}\mathbf{x}_0\right\|}_{\tau_k} + \underbrace{\frac{1}{c}\mathbf{v}_k^T \mathbf{u}_0}_{\dot{\tau}_k} \cdot t
\end{aligned} \tag{5}$$

[1] A similar analysis for moving sources and moving sensors also arrives at linear models.

where $\mathbf{\Delta x}_0$ is the distance vector from the source to sensor k, and $\mathbf{u}_0 \triangleq \frac{\mathbf{\Delta x}_0}{\|\mathbf{\Delta x}_0\|}$ is direction vector from the source to the sensor, and $\mathbf{v}_k^T \mathbf{u}_0$ is the component of the velocity in the direction of the source.

Throughout the document, a linear model for delay is used, as it allows for sums and differences of delays also to be expressed as linear in time.

$$\tau_k(t) = \tau_k + \dot{\tau}_k \cdot t \tag{6}$$

where $\dot{\tau}_k$ is unit-less and can be related to differential Doppler

$$\begin{aligned} \dot{\delta} &= \frac{1}{c}\frac{d\,\text{Range}}{dt} = \frac{\lambda_c}{c}\,\text{Doppler} \\ \text{f}_c\dot{\delta} &= \text{Doppler} \end{aligned}$$

where λ_c is the wavelength at the center frequency f_c.

2.2 NOTATION

Defining the receive waveform without noise and without the amplitude and phase scaling $\mathbf{r}_k$, Eqn. (2) can be written as

$$z_k[l] = a_k e^{j\phi_k} \underbrace{e^{-j2\pi \text{f}_0\, c\, \tau_k(t_l)}\, s(t_l - (t_s + \tau_k(t_l)))}_{r_{k,l}} + \nu_k(t_l) \tag{7}$$

$$= \underbrace{a_k e^{j\phi_k}}_{\triangleq b_k} r_{k,l}(\boldsymbol{\theta}) + \nu_k(t_l) \tag{8}$$

where the waveform without noise is parametrized by $\boldsymbol{\theta}$ containing the source parameter of interest $\mathbf{x}_0$ and unknown nuisance parameters

$$\boldsymbol{\theta} = \Big(\underbrace{t_s, a_1, a_2, \ldots, a_K,\, \phi_1, \phi_2, \ldots, \phi_K}_{\text{real nuisance parameters}}, \mathbf{x}_0\Big) \tag{9}$$

$$= \Big(t_s, b_1, b_2, \ldots, b_K, \mathbf{x}_0\Big) \tag{10}$$

In vector notation, the $1 \times L$ samples over time for each platform can be written as

$$\mathbf{z}_k = b_k \mathbf{r}_k(\boldsymbol{\theta}) + \boldsymbol{\nu}_k, \tag{11}$$

where

$$\mathbf{z}_k = \begin{pmatrix} z_k(t_0) \\ z_k(t_1) \\ \vdots \\ z_k(t_{L-1}) \end{pmatrix}^T, \boldsymbol{\nu}_k = \begin{pmatrix} \nu_k(t_0) \\ \nu_k(t_1) \\ \vdots \\ \nu_k(t_{L-1}) \end{pmatrix}^T, \mathbf{r}_k(\boldsymbol{\theta}) = \begin{pmatrix} r_{k,0}(\theta) \\ r_{k,1}(\theta) \\ \vdots \\ r_{k,L-1}(\theta) \end{pmatrix}^T \tag{12}$$

Finally, the observations from the K different platforms can be stacked in a $K \times L$ matrix form to allow for a compact notation of the entire KL measurements

$$\mathbf{Z} = \begin{pmatrix} \mathbf{z}_1 \\ \vdots \\ \mathbf{z}_K \end{pmatrix} = \begin{pmatrix} b_1 \mathbf{r}_1(\theta) \\ \vdots \\ b_K \mathbf{r}_K(\theta) \end{pmatrix} + \begin{pmatrix} \boldsymbol{\nu}_1 \\ \vdots \\ \boldsymbol{\nu}_K \end{pmatrix} \tag{13}$$

2.3 MAXIMUM-LIKELIHOOD ESTIMATOR (KNOWN SINGLE SIGNAL)

For the observation model (11) with complex Gaussian noise, the probability distribution conditioned on the unknown parameters can be written as

$$p(\mathbf{z}_1, \ldots, \mathbf{z}_K | \boldsymbol{\theta}) = \left(\pi\sigma^2\right)^{-LK} \prod_{k=1}^{K} e^{-\frac{1}{\sigma^2}\|b_k \mathbf{z}_k - \mathbf{r}_k(\boldsymbol{\theta}_k)\|^2} \tag{14}$$

where $\boldsymbol{\theta}_k = (\mathbf{x}_0, a_k, \phi_k)$. When the signal $s(t)$ is known, the received signals $\mathbf{r}_k$ can be computed for a given (time-varying) delay, and the maximum likelihood (ML) estimator reduces to a correlator. This can be shown by solving for the unknown amplitudes and phases by maximizing the likelihood, and completing squares in the likelihood function to simplify. Details of this calculation are shown in the next section for the two signal case.

$$\boldsymbol{\theta}_{\mathrm{ML}} = \arg\max_{\boldsymbol{\theta}} p(\mathbf{Z}|\boldsymbol{\theta}) \tag{15}$$

$$\mathbf{x}_{\mathrm{ML}} = \arg\max_{\mathbf{x}_0} \Big\{ \prod_{k=1}^{K} \exp\Big(\frac{1}{d_k\, \sigma^2} \underbrace{\left|\mathbf{z}_k \mathbf{r}_k^H\right|^2}_{\text{correlator}} \Big) \Big\} \tag{16}$$

Assuming that the delayed signals at each sensor have approximately the same norm $d \approx d_k = \|\mathbf{r}_k\|^2$,

$$\boxed{\mathbf{x}_{\mathrm{ML}} = \arg \max_{\boldsymbol{\tau}(t), t_s} \Big\{ \sum_{k=1}^{K} \left|\mathbf{z}_k \mathbf{r}_k^H\, (\tau_k(t), t_s)\right|^2 \Big\}} \tag{17}$$

where $\boldsymbol{\tau}(t) = (\tau_1(t), \ldots, \tau_K(t))$ are the (time-varying) delays for a hypothesis $\mathbf{x}_0$ position, and the argument of $\mathbf{r}_k$ has been called out explicitly. The same result has been obtained for the continuous time case with delays only in [1, Eqn.(21)], and is well known.

2.4 MAXIMUM-LIKELIHOOD ESTIMATOR (KNOWN TWO SIGNALS)

When two signals are present, the parameter estimates for the signals must be determined jointly since the signals may be correlated. Consider the received signal written in terms of samples, and in vector form as

$$z_k[l] = b_{k,1}\, r1_{k,l} + b_{k,2}\, r2_{k,l} + \nu_k(t_l) \tag{18}$$

$$\mathbf{z}_k = b_{k,1}\, \mathbf{r1}_k + b_{k,2}\, \mathbf{r2}_k + \boldsymbol{\nu}_k \tag{19}$$

Writing the sum of the signals in matrix form will allow for a simple expression for the ML estimate

$$\mathbf{z}_k = \boldsymbol{\beta}_k \mathbf{S}_k + \boldsymbol{\nu}_k \tag{20}$$

where $\mathbf{r1}, \mathbf{r2}$ are signals from different sources, possibly using the same pulse waveform, same symbol rate, and same preamble bits, and

$$\boldsymbol{\beta}_k = [b_{k,1}\ b_{k,2}] \tag{21}$$

$$\mathbf{S}_k = \begin{bmatrix} \mathbf{r1}_k \\ \mathbf{r2}_k \end{bmatrix} \tag{22}$$

The joint likelihood for the parameters $\boldsymbol{\theta} = \Big(t_{s,1}, b_{1,1}, b_{2,1}, \ldots, b_{K,1}, \mathbf{x}_{0,1}, t_{s,2}, b_{1,2}, b_{2,2}, \ldots, b_{K,2}, \mathbf{x}_{0,2}\Big)$ for both signals is

$$\begin{aligned} p(\mathbf{z}_1, \ldots, \mathbf{z}_K|\boldsymbol{\theta}) &= \left(\pi\sigma^2\right)^{-LK} \prod_{k=1}^{K} e^{-\frac{1}{\sigma^2}\left\|\mathbf{z}_k - b_{k,1}\mathbf{r1}_k(\boldsymbol{\theta}_k) - b_{k,2}\mathbf{r2}_k(\boldsymbol{\theta}_k)\right\|^2} \\ &= \left(\pi\sigma^2\right)^{-LK} \prod_{k=1}^{K} e^{-\frac{1}{\sigma^2}\mathrm{tr}\left\{\left(\mathbf{z}_k - \boldsymbol{\beta}\,\mathbf{S}_k\right)\left(\mathbf{z}_k - \boldsymbol{\beta}\,\mathbf{S}_k\right)^H\right\}} \end{aligned} \tag{23}$$

where $\mathrm{tr}\{\cdot\}$ is the trace of a matrix, or the sum of the diagonal entries.

The ordinary least-squares problem for the unknown complex scalars $\boldsymbol{\beta}$ can be solved by completing the square. Similar derivation can be found in [2] and [3, p.109]

$$\begin{aligned} \mathrm{tr}\left\{\left(\mathbf{z}_k - \boldsymbol{\beta}\,\mathbf{S}_k\right)\left(\mathbf{z}_k - \boldsymbol{\beta}\,\mathbf{S}_k\right)^H\right\} &= \mathrm{tr}\left\{\left(\boldsymbol{\beta}\,\mathbf{S}_k - \mathbf{z}_k\right)\left(\boldsymbol{\beta}\,\mathbf{S}_k - \mathbf{z}_k\right)^H\right\} \\ &= \mathrm{tr}\Big\{\left(\boldsymbol{\beta} - \mathbf{z}_k\mathbf{S}_k^H(\mathbf{S}_k\mathbf{S}_k^H)^{-1}\right)\left(\mathbf{S}_k\mathbf{S}_k^H\right)\left(\boldsymbol{\beta} - \mathbf{z}_k\mathbf{S}_k^H(\mathbf{S}_k\mathbf{S}_k^H)^{-1}\right)^H \\ &\quad - \mathbf{z}_k\mathbf{S}_k^H(\mathbf{S}_k\mathbf{S}_k^H)^{-1}\mathbf{S}_k\mathbf{z}_k^H + \mathbf{z}_k\mathbf{z}_k^H\Big\} \\ &= \mathrm{tr}\Big\{\left(\boldsymbol{\beta} - \mathbf{z}_k\mathbf{S}_k^H(\mathbf{S}_k\mathbf{S}_k^H)^{-1}\right)\left(\mathbf{S}_k\mathbf{S}_k^H\right)\left(\boldsymbol{\beta} - \mathbf{z}_k\mathbf{S}_k^H(\mathbf{S}_k\mathbf{S}_k^H)^{-1}\right)^H \\ &\quad - \mathbf{z}_k\left[\mathbf{I} - \mathbf{S}_k^H(\mathbf{S}_k\mathbf{S}_k^H)^{-1}\mathbf{S}_k\right]\mathbf{z}_k^H\Big\} \\ &= \mathrm{tr}\left\{\underbrace{\left(\boldsymbol{\beta} - \mathbf{z}_k\mathbf{S}_k^+\right)\left(\mathbf{S}_k\mathbf{S}_k^H\right)\left(\boldsymbol{\beta} - \mathbf{z}_k\mathbf{S}_k^+\right)^H}_{\text{quadratic term}} + \mathbf{z}_k\mathbf{P}_{\mathbf{S}_k}^{\perp}\mathbf{z}_k^H\right\} \end{aligned} \tag{24}$$

where $\mathbf{P}_{\mathbf{S}_k}^{\perp} = \left[\mathbf{I} - \mathbf{S}_k^H(\mathbf{S}_k\mathbf{S}_k^H)^{-1}\mathbf{S}_k\right] \in \mathbb{C}^{2\times 2}$ is the projection matrix for the null-space of $\mathbf{S}_k$, and the pseudo-inverse is defined as

$$\mathbf{S}_k^+ = \mathbf{S}_k^H\ \left(\mathbf{S}_k\,\mathbf{S}_k^H\right)^{-1} \in \mathbb{C}^{L\times 2} \tag{25}$$

The derivation assumes that the cross-correlation matrix between the reference signals ($\mathbf{S}_k\mathbf{S}_k^H$) has full rank of two, so that its inverse exists.

From (24), the optimal estimate for $\boldsymbol{\beta}$ that zeros out the quadratic term in the trace is

$$\widehat{\boldsymbol{\beta}} = \mathbf{z}_k \, \mathbf{S}_k^{+} = \mathbf{z}_k \, \mathbf{S}_k^H \, \left(\mathbf{S}_k \, \mathbf{S}_k^H \right)^{-1} \tag{26}$$

Plugging in this estimate into (24) reduces the maximum likelihood estimate to minimizing the sum of the residuals between the measurements and the model for each hypothesis position

$$\{\mathbf{x}_{0,1}, \mathbf{x}_{0,2}\}_{\mathrm{ML}} = \arg\min \Big\{ \sum_{k=1}^{K} \mathbf{z}_k \mathbf{P}_{\mathbf{S}_k}^{\perp} \mathbf{z}_k^H \Big\} \tag{27}$$

A more intuitive way to write the result is

$$\boxed{\{\mathbf{x}_{0,1}, \mathbf{x}_{0,2}\}_{\mathrm{ML}} = \arg \max_{\boldsymbol{\tau}1(t), t_{s,1}, \boldsymbol{\tau}2(t), t_{s,2}} \Big\{ \sum_{k=1}^{K} \Big\| \mathbf{z}_k \mathbf{S}_k^H \left(\mathbf{S}_k \mathbf{S}_k^H \right)^{-\frac{1}{2}} \Big\|^2 \Big\}} \tag{28}$$

where the dependency of the signal template matrix $\mathbf{S}_k$ on the hypothesis position can be called out explicitly

$$\mathbf{S}_k(t_{s,1}, \tau 1_k(t), t_{s,2}, \tau 2_k(t)) \tag{29}$$

The metric involves the whitening term $\left(\mathbf{S}_k \mathbf{S}_k^H \right)^{-\frac{1}{2}}$ applied to the signal matrix before correlating with the sensor measurements. Comparing (28) with (17), it is possible to see how the two signal case simplifies to the one signal case. When the two signals are uncorrelated leading to a diagonal $\left(\mathbf{S}_k \mathbf{S}_k^H \right)^{-\frac{1}{2}}$, the ML solution separates into independent solutions for each signal.

Because of the complexity of the search for multiple signals that are correlated [2], the maximum likelihood approach has often been replaced with cross-correlation approaches, and more recently subspace approaches.

2.5 MAXIMUM LIKELIHOOD ESTIMATOR (UNKNOWN SINGLE SIGNAL, NO DOPPLER)

It is easier to work with Gaussian signals in continuous time when considering unknown signals. The ML estimate for TDOA geolocation for discrete time was first described in [5] where the term direct position determination (DPD) technique was coined. The DPD technique jointly solves for position using the sensor measurements and differs from conventional two-step techniques that estimate delay and then solve for position. As a result, for sparse sensors, the transfer of sensor measurements introduces a communication overhead or bandwidth expansion of K. A more thorough continuous-time analysis for real signals is shown in [1] using Fourier series.

It is assumed here that the signal duration is sufficiently short, so that Doppler frequency shift induced by the motion of the sensors or the source, is negligible. A significant Doppler shift

[2] An approach for considering one signal at a time is presented in [4, Sec.3.2.2].

destroys the assumption of independent frequency components that makes the analysis in this section possible.

Consider the continuous time receive model due to a transmitted signal $s(t)$ going through a channel $h_k(t)$ particular to each sensor, and noise $\nu_k(t)$ added at each sensor

$$z_k(t) = \int_{-\infty}^{\infty} s(t-\zeta)\, h_k(\zeta)\, d\zeta + \nu_k(t) \tag{30}$$

where the integral represents convolution of the signal with the channel. In the frequency domain, the equivalent relationship is

$$z_k(\omega) = s(\omega)h_k(\omega) + \nu_k(\omega) \tag{31}$$

where by an abuse of notation, it will be clear whether the signals, channel, and noise are time domain or frequency domain based on their arguments.

Model the signal and noise as zero-mean circularly symmetric complex Gaussian variables, independent over frequency with covariance

$$\mathbb{E}\left\{s(\omega)s^*(\omega)\right\} \triangleq S(\omega) \tag{32}$$

$$\mathbb{E}\left\{\nu_k(\omega)\nu_l^*(\omega)\right\} \triangleq \sigma^2 \mathbb{1}_{k,l} \tag{33}$$

where $\mathbb{1}_{k,l}$ is the indicator function that evaluates to one when $k = l$, the noise power σ^2 is flat, and the signal power S which varies over frequency will later be assumed to be flat. The received signal is then Gaussian with covariance

$$\mathbb{E}\left\{z_k(\omega)\, z_l^*(\omega)\right\} = S(\omega)h_k(\omega)h_l^*(\omega) + \sigma^2 \mathbb{1}_{k,l} \tag{34}$$

Consolidate the K sensor spectra and channel response correlations as

$$\mathbf{z} = \begin{bmatrix} z_1(\omega) \\ \vdots \\ z_K(\omega) \end{bmatrix}, \mathbf{h} = \begin{bmatrix} h_1(\omega) \\ \vdots \\ h_K(\omega) \end{bmatrix}, \mathbf{H}(\omega) = \mathbf{h}(\omega)\mathbf{h}(\omega)^H \tag{35}$$

where the fact that $\mathbf{H}$ is rank one will enable simplification in the likelihood.

The joint probability density for all sensors observations at a given frequency is

$$p\left(\mathbf{z}(\omega)|\mathbf{H}(\omega), S(\omega)\right) = \pi^{-K} \left|\mathbf{\Sigma}(\omega)\right|^{-1} \exp\left\{-\mathbf{z}(\omega)^H \mathbf{\Sigma}(\omega)^{-1}\mathbf{z}(\omega)\right\} \tag{36}$$

where the ensemble covariance matrix from (34) is

$$\mathbf{\Sigma}(\omega) \triangleq S(\omega)\mathbf{H}(\omega) + \sigma^2\mathbf{I} \tag{37}$$

and $\mathbf{I}$ is the $K \times K$ identity matrix.

Using the matrix inversion lemma, the term in the exponent can be computed as

$$\sigma^2 \mathbf{z}(\omega)^H \mathbf{\Sigma}^{-1} \mathbf{z}(\omega) = \mathbf{z}(\omega)^H \left(\mathbf{I} - \frac{\frac{S(\omega)}{\sigma^2} \mathbf{h}(\omega)\mathbf{h}(\omega)^H}{1 + \frac{S(\omega)}{\sigma^2} \|\mathbf{h}(\omega)\|^2} \right) \mathbf{z}(\omega) \tag{38}$$

$$= \|\mathbf{z}(\omega)\|^2 - \frac{\frac{S(\omega)}{\sigma^2} \left| \mathbf{z}(\omega)^H \mathbf{h}(\omega) \right|^2}{1 + \frac{S(\omega)}{\sigma^2} \|\mathbf{h}(\omega)\|^2} \tag{39}$$

where the determinant of the ensemble covariance due to Sylvester's determinant identity is

$$|\mathbf{\Sigma}(\omega)| = K \left(S(\omega) \|\mathbf{h}(\omega)\|^2 + \sigma^2 \right) \tag{40}$$

The log likelihood can then be expressed as

$$\log p\left(\mathbf{z}(\omega)|\mathbf{H}(\omega), S(\omega)\right) = -K \log(\pi) - \log \left(K \left(S(\omega) \|\mathbf{h}(\omega)\|^2 + \sigma^2 \right) \right) - \frac{1}{\sigma^2} \left(\|\mathbf{z}(\omega)\|^2 - \frac{\frac{S(\omega)}{\sigma^2} \left| \mathbf{z}(\omega)^H \mathbf{h}(\omega) \right|^2}{1 + \frac{S(\omega)}{\sigma^2} \|\mathbf{h}(\omega)\|^2} \right) \tag{41}$$

Due to the independence across frequency, the log likelihoods are additive and the maximum likelihood solution is computed as

$$\max_{\mathbf{H}(\omega)} \int \log p\left(\mathbf{z}(\omega)|\mathbf{H}(\omega), S(\omega)\right) d\omega \tag{42}$$

where the integral is over the bandwidth of the signal. Retaining the relevant terms of the likelihood, the expression to be maximized is

$$\max_{\mathbf{h}(\omega)} \int \log \left(\widetilde{S}(\omega) \|\mathbf{h}\|^2 + 1 \right) + \frac{1}{\sigma^2} \frac{\widetilde{S}(\omega) \left| \mathbf{h}^H(\omega)\mathbf{z}(\omega) \right|^2}{1 + \widetilde{S}(\omega) \|\mathbf{h}(\omega)\|^2} d\omega \tag{43}$$

where $\widetilde{S}(\omega) = \frac{S(\omega)}{\sigma^2}$ is the normalized signal power.

Consider a gain and delay model without multi-path for the channel

$$h_k(t) = g_k \mathbb{1}(t - \tau_k(\mathbf{x}_0)) \rightarrow h_k(\omega) = g_k e^{-j\omega\tau_k(\mathbf{x}_0)} \tag{44}$$

where τ_k is the hypothesis delay for sensor k, but g_k is a unknown complex gain scalar, and $\mathbb{1}$ is used here as the Dirac-delta function instead of the indicator function. It may be possible to impose a line-of-sight model to obtain g_k for a given hypothesis position, but such an approach is sensitive to the gains and antenna at each sensor, and so is not adopted here. The relevant term in the likelihood that involves the correlations between the sensors is

$$\left| \mathbf{h}^H(\omega)\mathbf{z}(\omega) \right|^2 = \sum_k \sum_l g_k^* g_l \underbrace{e^{j\omega(\tau_k(\mathbf{x}_0) - \tau_l(\mathbf{x}_0))} z_k(\omega) z_l^*(\omega)}_{\triangleq \Gamma_{k,l}(\omega, \mathbf{x}_0)} \tag{45}$$

$$= \mathbf{g}^H \mathbf{\Gamma}(\omega, \mathbf{x}_0)\, \mathbf{g} \tag{46}$$

where the $K \times K$ matrix $\mathbf{\Gamma}(\omega, \mathbf{x}_0)$ depends on frequency and source position, but the unknown gains of the channel are fixed over frequency. Since the source position is unknown, $\mathbf{x}_0$ is treated as a source position hypothesis to be tested.

A simplification that is particularly useful is when the signal of interest has a flat spectrum over some known bandwidth B. In this case, the maximization can be written as

$$\max_{\mathbf{g}} \; -2\pi B \log\left(1 + \widetilde{S}\,\|\mathbf{g}\|^2\right) + \frac{1}{\sigma^2}\frac{\widetilde{S}\,\mathbf{g}^H \mathbf{\Gamma}(\mathbf{x}_0)\,\mathbf{g}}{1 + \widetilde{S}\,\|\mathbf{g}\|^2} \tag{47}$$

where $\mathbf{\Gamma}(\mathbf{x}_0) = \int \mathbf{\Gamma}(\omega, \mathbf{x}_0) d\omega$ is the pairwise sensor correlations integrated over frequency. It may be possible to show that this maximization is monotonic in the eigenvalue problem for $\mathbf{\Gamma}(\mathbf{x}_0)$. A simpler route is to consider the maximization in two steps as follows

$$\max_{\alpha} \; -2\pi B \log(1 + \widetilde{S}\alpha) + \frac{1}{\sigma^2}\frac{\widetilde{S}}{1 + \widetilde{S}\alpha}\Big(\max_{\mathbf{g}, \|\mathbf{g}\|^2 = \alpha} \mathbf{g}^H \mathbf{\Gamma}(\mathbf{x}_0)\,\mathbf{g}\Big) \tag{48}$$

$$= \max_{\alpha} \; -2\pi B \log(1 + \widetilde{S}\alpha) + \frac{1}{\sigma^2}\frac{\widetilde{S}}{1 + \widetilde{S}\alpha}\Big(\alpha\,\lambda_{\max}\left\{\mathbf{\Gamma}(\mathbf{x}_0)\right\}\Big) \tag{49}$$

where the maximization of the norm $\mathbf{g}^H \mathbf{\Gamma}(\mathbf{x}_0)\mathbf{g}$ subject to a linear constraint has been recognized as an eigenvalue problem and $\lambda_{\max}$ is the largest (principal) eigenvalue. Finally, using simple calculus, the maximization over the constraint α yields

$$\alpha = \frac{\frac{\lambda_{\max}}{\sigma^2} - 2\pi B}{\widetilde{S}\left(\lambda_{\max}\left(1 - \frac{1}{\sigma^2}\right) + 2\pi B\right)} \tag{50}$$

where the requirement that $\alpha > 0$ for arbitrarily and without loss of generality $\sigma^2 \geq 1$ implies that the solution is valid when

$$\frac{\lambda_{\max}}{\sigma^2} > 2\pi B \tag{51}$$

Comparing the elements of $\mathbf{\Gamma}(\mathbf{x}_0)$ with (34) for the gain and phase channel model, the diagonals are the sum of signal and noise power at each sensor

$$\text{diagonals } \mathbf{\Gamma}_{k,k}(\mathbf{x}_0) : \mathbb{E}\left\{\int_{\omega} \|z_k(\omega)\|^2 \, d\omega\right\} = 2\pi B\,\left(S\,|g_k|^2 + \sigma^2\right) \tag{52}$$

Since these entries are least as large as $\sigma^2 \geq 1$, the integration over frequency (which multiples by $2\pi B$) guarantees (51). The off-diagonal elements of $\mathbf{\Gamma}(\mathbf{x}_0)$ can be shown to have a sinc $\triangleq \sin(x)/x$ shape

$$\text{off-diagonals } \mathbf{\Gamma}_{k,l}(\mathbf{x}_0) : \mathbb{E}\left\{\int_{\omega} e^{j\omega(\tau_k(\mathbf{x}_0) - \tau_l(\mathbf{x}_0))} z_k(\omega)\, z_l^*(\omega) d\omega\right\}$$
$$= 2\pi B\, S g_k\, g_l^* \text{sinc}\left(\pi B\, \delta_{k,l}(\mathbf{x}_0)\right) \tag{53}$$

where $\delta_{k,l}(\mathbf{x}_0) = (\tau_k(\mathbf{x}_0) - \tau_l(\mathbf{x}_0)) - (\tau_k(\mathbf{x}_{0,\text{true}}) - \tau_l(\mathbf{x}_{0,\text{true}}))$ evaluates to zero at the true source position, maximizing the sinc at one.

Although the ML solution computed here involves plugging α from (50) into (49), the principal eigenvalue of $\mathbf{\Gamma}(\mathbf{x}_0)$ can often itself be used as the metric due to monotonicity arguments. Summarizing the result, for a given hypothesis position and corresponding delays, the principal eigenvalue represents how well the observed signals can be aligned across sensors and across frequency using a complex scalar at each sensor

$$\boxed{\begin{aligned} \mathbf{x}_{\text{ML}} &= \arg\max_{\mathbf{x}_0} \lambda_{\max}\left\{\mathbf{\Gamma}(\mathbf{x}_0)\right\} && \text{(54a)} \\ \mathbf{\Gamma}_{k,l}(\mathbf{x}_0) &\triangleq \int e^{j\omega(\tau_k(\mathbf{x}_0)-\tau_l(\mathbf{x}_0))} z_k(\omega) z_l^*(\omega) d\omega && \text{(54b)} \end{aligned}}$$

The principal eigenvector $\mathbf{e}_{\max}\left\{\mathbf{\Gamma}(\mathbf{x}_0)\right\}$ is the value of the complex scalar alignments and may also account for any mismatched sensors by giving them less weight in the metric.

Efficiently implementing the proposed metric for discrete-time signals would involve computing the Fast-Fourier Transform (FFT) over a block of samples L, and introducing a linear phase ramp for each sensor based on the hypothesis position. For this purpose, define the the FFT of the hypothesis shifted observations as

$$(\mathbf{Z}_{\mathbf{x}_0})_{k,m} \triangleq z_k(\omega_m) e^{j\omega_m \tau_k(\mathbf{x}_0)} \tag{55}$$

where $\omega_m = 2\pi m/L$ is the discrete frequency, and $(\mathbf{Z}_{\mathbf{x}_0})_{k,m}$ is the m-th FFT bin for sensor k. Then, the discrete form of the correlations matrix, with entries written out is

$$\mathbf{\Gamma}(\mathbf{x}_0) = \mathbf{Z}_{\mathbf{x}_0}\mathbf{Z}_{\mathbf{x}_0}^H \tag{56}$$

$$= \sum_{m=0}^{L-1} \begin{bmatrix} \|z_1(\omega_m)\|^2 & z_1 z_2^* e^{j\omega_m(\tau_1(\mathbf{x}_0)-\tau_2(\mathbf{x}_0))} & \cdots \\ z_1^* z_2 e^{j\omega_m(\tau_2(\mathbf{x}_0)-\tau_1(\mathbf{x}_0))} & \|z_2(\omega_m)\|^2 & \\ \vdots & & \ddots \\ & & \|z_K(\omega_m)\|^2 \end{bmatrix} \tag{57}$$

where the terms z_k are functions of ω_m but not shown in the expression (57) for compactness.

3. UNKNOWN MULTIPLE SIGNALS OVERVIEW

The primary concern of this report is source position estimates in the presence of interference, that is, the multiple signals scenario where some of the signals are unknown. In this section, various approaches are proposed and briefly described. The rest of the report goes into extensive detail on the approaches and gives some salient examples. Many of the approaches are simply a function of the covariance matrix $\mathbf{\Gamma}(\mathbf{x}_0)$.

1. **Cross Correlation** The traditional approach for addressing unknown multiple signals is cross correlation. The approach has widespread use, and is sometimes referred to as a radiometer for the two-element case where it has been used as a constant-false-alarm rate (CFAR) detector. The approach is to take the sum of the magnitude of the upper (or lower) off-diagonal elements in the matrix $\mathbf{\Gamma}(\mathbf{x}_0)$ and divide by its trace, leading to (in the mean) a sinc response in the geolocation metric

$$\frac{\mathbb{E}\left\{\sum_k \sum_{l>k} |\mathbf{\Gamma}_{k,l}(\mathbf{x}_0)|\right\}}{\mathbb{E}\left\{\sum_k |\mathbf{\Gamma}_{k,k}(\mathbf{x}_0)|\right\}} = \frac{S\sum_k \sum_{l>k} g_k g_l^* \mathrm{sinc}\left(\pi B\, \delta_{k,l}(\mathbf{x}_0)\right)}{K\sigma^2 + S\sum_k |g_k|^2} \tag{58}$$

   The resolution of the technique is often thought to be $\frac{1}{B}$ since the sinc response drops to zero when $\tau_{k,l}(\mathbf{x}_0)$ is shifted from the true position by $\frac{1}{B}$. However, the side-lobes of the sinc should be considered, and, as is shown in Section 4, the side-lobes of a signal due to cyclostationarity of the communications waveform limit resolution when multiple signals are present.

2. **Wideband AEP** Referring to the ML approaches, one way to treat the multiple signal scenario is to whiten the measured covariance in (37), so that the whitened measurements can then be treated the same way as in the single signal scenario, leading to a eigenvalue metric for combining the whitened covariances over frequency. A background covariance without the signal of interest can be measurerd either before the signal of interest turns on or after the signal of interest turns off. In the framework of detection, this leads to an approach called adaptive event processing (AEP) [3, p.112-114]. Stationarity of the background is important here as changes in the estimated covariances would lead to a false contrast.

Consider the example shown in Figure 3, where the traditional cross correlation approach would provide better estimates for signal 1 and signal 2 when computed in the absence of the larger, interference signal. A detection approach could be used to find the start and end of signals, allowing for better intervals for computing cross correlation. In the whitening approach, a background covariance estimated using a sliding window could be used to remove the interference signal.

3. **Wideband MUSIC** An alternative to whitening approaches is to consider a wideband analogue to the narrowband MUSIC direction finding approach. Here, an estimate of the signal subspace and a hypothesis signal model at each frequency are used to separate the signals simultaneously present (instead of processing an optimal interval of the time measurements).

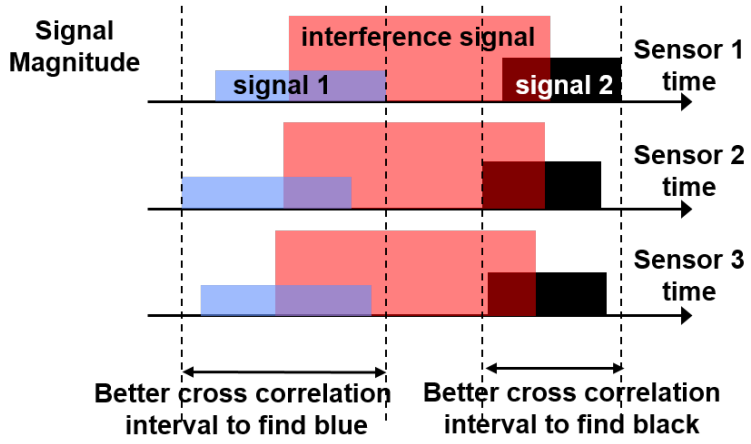

Figure 3. Example scenario for differing power signals turning on and off at different times. A cross-correlation technique using the entire time interval may fail due to a large interference signal; whereas, better time intervals are possible. Alternatively, since the time interval has on and off transitions, a sliding whitening detector can be used to estimate delay.

Consider a covariance estimate for each frequency (instead of the covariance estimate integrated over frequency) obtained through frequency channelization instead of through an FFT. Each frequency channel has time samples to allow for an estimate of the spatial covariance and corresponding signal and noise subspaces. Then, a MUSIC metric for each channel would consider distance from a modeled steering vector evaluated at the channel center frequency to the estimated signal subspace. Combining the distance metric over the frequency channels while accounting for a unknown gain and phase at each sensor (fixed over frequency) results in a eigenvalue problem very similar to (54a).

4. **Wideband Demod/Remod** For communications signals with a known preamble, the entire waveform could be estimated through adaptive beamforming focused using the preamble in a minimum mean-squared error (MMSE) sense. Since the waveform in this setting is partially known, it is possible to use symbol decisions and the known modulation to iteratively update the beamforming over time to account for Doppler, and in some cases to account for new signals appearing in the environment. Two well-established approaches for beamforming to mitigate delay spread across the sensors are space-time adaptive processing (STAP) using time taps [6, Fig.22] and using frequency channelization [6, Fig.39]. In this report, the frequency channelization architecture is pursued due to a simple efficient implementation.

4. CROSS CORRELATION APPROACH

Despite the need for long sequence lengths to obtain delay estimates for signals of differing powers, cross correlation techniques are widely used in geolocation. Algebraic techniques [**?**, 7–10] rely on delay estimates obtained from cross correlation peaks, whereas imaging techniques evaluate a likelihood over a hypothesis position grid. The algebraic techniques or so-called two-step techniques have been shown to be worse in performance at low SNRs compared to so-called direct positioning techniques [1, 11]. Since algebraic techniques rely on approximations or assumptions to convert the nonlinear geolocation problem to linear or quadratic form, they typically need an extra sensor measurement in order to provide a solution. Imaging techniques are often used for 2-dimensional search due to tractability. These techniques also allow for multiple sources to be located simultaneously without the necessity of pairing the delay estimates as is needed for the algebraic techniques.

Consider the cross-correlation approach in more depth by examining the ambiguity function of a waveform, and its sidelobes. The ambiguity function for the waveform, or more generally, the cross-ambiguity function (CAF) between the signal $s_1(t)$ and the signal $s_2(t)$ is the correlation between these signals as they are shifted in time and frequency. The CAF $\rho(\tau, \nu)$ where τ is the relative time delay and $\nu = f_2 - f_1$ is the relative frequency offset is defined as

$$\rho(\tau,\nu) = \langle s_1(t+\tau_d)\exp(j2\pi f_1(t+\tau_d)),\, s_2(t)\exp(j2\pi f_2 t)\rangle \tag{59}$$

$$= \exp(j2\pi f_1\tau_d)\,\exp(j2\pi f_2\tau)\int_{-\infty}^{\infty} s_1(t+\tau_d)\,s_2^*(t-\tau)\exp(j2\pi(f_1-f_2)t)\,dt \tag{60}$$

$$= \exp(j2\pi f_1\tau_d)\,\exp(j2\pi f_2\tau)\int_{-\infty}^{\infty} s_1(t)\,s_2^*(t-\tau)\exp(-j2\pi\nu t)\,dt \tag{61}$$

$$|\rho(\tau,\nu)|^2 = \left|\int_{-\infty}^{\infty} s_1(t)\,s_2^*(t+\tau)\exp(j2\pi\nu t)\,dt\right|^2 \tag{62}$$

For a given signal $s(t)$, the ambiguity function is maximized at zero delay and zero frequency offset. At delays greater than one symbol length, extrema in the ambiguity function contribute to a side lobe level (that potentially prevents other signals from being detected and estimated). Primarily, the side lobe level depends on the correlation between the samples of the discrete sequence $b[n]$, as will be shown next for delays only. A result in this setting is that the maximum of the correlation of random binary sequences tends to $\sqrt{B}$, where B is the sequence length [12].

Consider the delay only autocorrelation of a BPSK signal with random bits $b[n] \in \{-1, 1\}$

$$\max_{|\tau|>T_c} \left|\int s(t)\,s^*(t+\tau)dt\right| \tag{63}$$

$$= \max_{|\tau|>T_c} \left|\int e^{j2\pi \mathrm{f}_0 t}\sum_n b[n]\,p(t-nT_c)\cdot e^{-j2\pi \mathrm{f}_0(t+\tau)}\sum_m b[m]\,p^*(t+\tau-mT_c)dt\right| \tag{64}$$

$$= \max_{|\tau|>T_c} \left|\int \sum_{n,m} b[n]\,b[m]\,p(t-nT_c)\,p^*(t+\tau-mT_c)dt\right| \tag{65}$$

For bandlimited pulses, the integral is maximized at delays τ that are multiples of the symbol rate. Making use of the result for random binary sequences, for the unit energy pulse, the side lobe level at $\tau = kT_c$ then becomes bounded as

$$B^{\frac{1-\epsilon}{2}} < \max \left| \sum_n b[n]\, b[n+k] \right| < B^{\frac{1+\epsilon}{2}} \tag{66}$$

where $\epsilon > 0$ depends on the sequence and in particular $\epsilon = 0$ (the bound is tight) for Barker sequences.

Consider two overlapping signals $A_1 s_1(t) + A_2 s_2(t - t_2)$ and the corresponding peaks and sidelobes in the ambiguity function resulting from self terms and cross terms. Expressions for the correlation due to frequency offset are hard to obtain, so the focus here is on delay

$$\rho(\tau) = \left| \int \Big(A_1 s_1(t) + A_2 s_2(t - t_2) \Big) \Big(A_1^* s_1^*(t + \tau) + A_2^* s_2^*(t - t_2 + \tau) \Big) dt \right| \tag{67}$$

Based on the single signal bound, the relevant maximum terms are

$$\text{self terms:} \quad |A_1|^2 B_1,\ |A_2|^2 B_2 \tag{68}$$

$$\text{sidelobe terms:} \quad |A_1|^2 \sqrt{B_1},\ |A_2|^2 \sqrt{B_2},\ \left| A_1 A_2^* \sqrt{\text{overlap between } B_1, B_2} \right| \tag{69}$$

$$\text{cross term:} \quad \left| A_1 A_2^* \sqrt{\text{overlap between } B_1, B_2} \right| \tag{70}$$

For the smaller signal (arbitrarily, $A_2 < A_1$) to appear above the sidelobe of the larger signal, assuming both are persistent $B_1 = B_2 = B$ and completely overlapped, the sequence length has to satisfy $\sqrt{B} > \frac{A_1^2}{A_2^2}$. For example, a 10 dB larger power signal would require $B = 2 *$ (10 dB + 5 dB margin above sidelobes) = 30 dB implying a sequence of length B=1000 for both signals.

4.1 RESISTIVE COMBINING METRIC

Cross-correlation techniques can be sensitive to differences in magnitude of the pairwise correlations, so that in the multiple signals setting, some lower power signals are obscured. An empirically validated technique that was found to be robust [13, 14], [15, Eqn.13] in the narrowband angle of arrival context as well as the TDOA context is to use resistive combining of the pairwise correlations, akin to minimum variance distortionless response (MVDR). The MVDR spectrum is computed as

$$P(\theta) = \frac{1}{[\text{spatial vector}(\theta)]^H \, (\text{spatial covariance})^{-1} \, [\text{spatial vector}(\theta)]} \tag{71}$$

where θ is the parameter of interest, taken to be $\theta = (x, y)$ position in the TDOA context. For combining over pairwise correlation images, the vector of interest is a just an indicator function for a particular x, y position (coming from a set of delays evaluated for the position). Then, treating

each pairwise correlation as independent of the other pairs, the covariance over the delays for a particular x, y position is just the sum of the pairwise correlations. As a result, the MVDR pixel value P for position x, y is obtained from the correlation pixel value $P_{k,q}$ for the sensor pair k, q as

$$P(x,y) = \frac{1}{\sum_{k=1}^{K} \sum_{q=k+1}^{K} \left(P_{k,q}(x,y)\right)^{-1}} \tag{72}$$

where in the denominator, the inverse of the covariance has along its diagonal the inverse of each pixel due to the assumption of independence.

The effect of resistive combining compared to linear combining of the pixels, defined as

$$P(x,y) = \sum_{k=1}^{K} \sum_{q=k+1}^{K} P_{k,q}(x,y) \tag{73}$$

is that linear combining tends to be dominated by the sensors with the highest received powers, while resistive combining tends to favor agreement among all the sensors.

4.2 COMPUTATION

Computation of the CAF can be done efficiently for discrete time sequences using a FFT [16]. Since circular convolution is equivalent to multiplication in the FFT domain, zero padding the input samples up to the desired lag achieves linear convolution using an FFT. A variety of frequency weightings have been suggested to determine time delay in a ML sense [17]. These generalized cross correlation (GCC) techniques can be implemented directly in the FFT domain.

This page intentionally left blank.

5. WIDEBAND ARCHITECTURES FOR HANDLING DELAY SPREAD

Before describing in more depth the wideband AEP, MUSIC and demod / remod approaches, a discussion is presented here on how the delay model (44) is affected by delay spread over bandwidth and Doppler spread due to motion.

Treating the continuous time signal as independent in each frequency allowed breaking up the maximum likelihood solution into parts that can then be combined in a optimal way through the eigenvector of the covariance $\mathbf{\Gamma}(\mathbf{x}_0)$. For discrete time signals of finite duration, and signals not necessarily completely overlapped, the analysis is not as straight-forward.

For discrete-time signals, frequency resolution is limited to one over the duration of the signal, which may be unknown, along with an unknown start time. Fine frequency resolution may not be desirable in the multiple signals setting due to finite sample and low SNR issues in estimating a spatial covariance per frequency. Such covariance estimation is fundamental to the beamforming techniques outlined in Section 3. It is often sufficient to channelize in frequency to the extent that the signals can jointly be assumed to be narrowband. Some clarity on the definition of narrowband based on the achievable null depth is provided in 5.1.

Doppler frequency shift due to relative motion of the sensors, and any motion of the signals, is mitigated by considering short time segments over which the carrier phase does not vary significantly. Iterative demodulation of communications signals and carrier tracking are found to be effective means of handling Doppler over longer time periods.

When multiple signals are present, determining an architecture that can effectively beamform towards the signal of interest is a complicated algebraic problem in general. When time taps (frequency taps) are used to align a particular signal, other signals become misaligned, and so on. Because time delay and frequency offset do not commute, a non-commutative algebra where the order of operations is taken into account is used to determine the number and placement of time and frequency taps [18]; this detailed discussion is beyond the scope of this document.

5.1 NULL DEPTH

In this section, some arguments are presented for the number of frequency channels needed to achieve a given null depth. The achievable null depth of the proposed beamforming techniques is related to the eigenvalue spread in $\mathbf{\Gamma}(\omega, \mathbf{x}_0)$. The basis for the arguments are that parameter estimates for a secondary signal of x dB lower power than a primary signal could be obtained when the covariance containing only the primary signal has a second eigenvalue that is at least x dB smaller than the primary eigenvalue.

Consider extending the narrowband analysis for arrays in [19] to the sparse sensors problem. For sensors and signals that are not moving (no Doppler), eigenvalue spread is caused by the product of delay spread and channelized bandwidth. Narrower frequency bins and smaller delay spreads cause less eigenvalue spread and lead to lower null depths. A simple and experimentally verified model for eigenvalue spread is *a single zero bandwidth signal splitting into two equal-power zero bandwidth signals*, as shown in Figure 4.

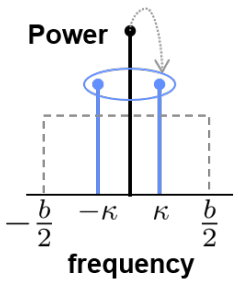

Figure 4. Signal over bandwidth b is modeled as a zero bandwidth signal (i.e., tone) splitting into two zero bandwidth signals at frequencies $\pm\kappa$ relative to the center. The split frequency κ is selected so that the original signal and the two tones have the same variance over frequency.

In a given frequency channel m, the spatial covariance formed from the signal measurements $\mathbf{y}_m$ over the K sensors and L time samples when a split occurs is

$$\mathbf{y}\mathbf{y}^H = S\mathbf{v}_1\mathbf{v}_1^H + S\mathbf{v}_2\mathbf{v}_2^H + \sigma^2\mathbf{I} \tag{74}$$

where $2S$ is the power of the signal before the split, and $\mathbf{v}_{1,2}$ are the steering vectors associated with split. The eigenvalues of the covariance $\mathbf{y}\mathbf{y}^H$ can be shown to be

$$\lambda_{1,2} = KS\left(1 \pm |\phi|\right) + \sigma^2 \tag{75}$$

where $|\phi|$ is the cosine of the angle between the two vectors $\mathbf{v}_1$ and $\mathbf{v}_2$

$$|\phi| \triangleq \frac{\mathbf{v}_1^H\mathbf{v}_2}{\|\mathbf{v}_1\|\,\|\mathbf{v}_2\|} \tag{76}$$

The ratio of second eigenvalue to the first eigenvalue can be defined as the achievable null depth

$$\boxed{\text{null depth} \triangleq \frac{\lambda_2}{\lambda_1} \underset{(S>>\sigma^2)}{\approx} \frac{1-|\phi|}{1+|\phi|}} \tag{77}$$

For the zero bandwidth signal pair, choose a frequency offset $\pm\kappa$ from the center of the bin that retains the variance over frequency [19, Eqn.22] compared with a signal that occupies the full channelized bandwidth of b. For a flat spectrum over this channelized bandwidth, this leads to a variance over frequency of $b^2/12$ which can be equated to the κ^2 variance of the split

$$\kappa^2 = \frac{b^2}{12} \tag{78}$$

For the narrowband signals, the steering vectors $\mathbf{v}_{1,2}$ are due to the delay model for the channel, and their cosine angle depends on the difference between the true delay and the delay due to the

hypothesis position $\mathbf{x}_0$

$$\mathbf{v}_{1,2} = e^{j(\omega_m \pm 2\pi\kappa)(\boldsymbol{\tau}(\mathbf{x_0}) - \boldsymbol{\tau}(\mathbf{x_0},\text{true}))} \tag{79}$$

$$|\phi| = \frac{1}{K}\left|\sum_k e^{j((\omega_m+2\pi\kappa)-(\omega_m-2\pi\kappa))\boldsymbol{\delta}}\right| \tag{80}$$

where $\delta_k(\mathbf{x}_0) = \tau_k(\mathbf{x}_0) - \tau_k(\mathbf{x}_{0,\text{true}})$. The cosine angle depends on the sensor positions, source position, and hypothesis position through the delays.

Assume that the delays are bounded as $(\boldsymbol{\tau}(\mathbf{x}_0) - \boldsymbol{\tau}(\mathbf{x}_{0,\text{true}})) \in (-\frac{\delta_{\max}}{2}, \frac{\delta_{\max}}{2})$ where $\delta_{\max}$ is called the delay spread. A simple upper bound on the cosine angle assumes that the delay is at the maximum value $\frac{\delta_{\max}}{2}$ for half the sensors and at negative this value for the other half. Another meaningful value for the cosine angle assumes that the delays are spaced uniformly at an interval of $\frac{\delta_{\max}}{K}$ over the delay spread

$$\begin{aligned} |\phi| &= \frac{1}{K}\left|\sum_k e^{j(2\pi\, 2\kappa)\delta_k}\right| \\ &\leq \cos\left(2\pi\,\frac{b}{\sqrt{3}}\,\frac{\delta_{\max}}{2}\right) &(81)\\ &\underset{\text{uniform}}{=} \frac{1}{K}\left|\frac{\sin\left(2\pi\,\frac{b}{\sqrt{3}}\,\frac{\delta_{\max}}{2}\right)}{\sin\left(\frac{1}{K}2\pi\,\frac{b}{\sqrt{3}}\,\frac{\delta_{\max}}{2}\right)}\right| &(82)\end{aligned}$$

where the ratio of $\sin(\cdot)/\sin(\cdot)$ produces a periodic sinc (Dirichlet) function with maximum of K. Figure 5 shows the predicted null depth as a function of the delay bandwidth product $b\,\delta_{\max}$. For a null depth of -20 dB, the prediction is that $\frac{1}{10}^{\text{th}}$ to $\frac{1}{5}^{\text{th}}$ sample split is required either through time of frequency taps. There is not a strong dependence of the null depth on the number of sensors K (and in fact the null depth is worse as the number of sensors increases), the way it is shown here. In reality, as the number of sensors increases, a portion of the sensors, and their associated delay spread could be used to accomplish the task of nulling, assuming that there are enough degrees of freedom available when multiple signals are present.

The approach considered here for delay spread does not readily extend to Doppler spread where the steering vectors $\mathbf{v}$ vary over time. While justification is not provided here [18, Eqn.14], an argument can be made that the effect of Doppler spread can be determined by replacing the delay bandwidth product in the sinc or cos expressions with

$$b\,\delta_{\max} \rightarrow T\text{f}_c\dot{\delta}_{\max} = T \cdot \text{differential Doppler} \tag{83}$$

where T is the integration time. For many scenarios of interest, the delay bandwidth product exceeds the time doppler product and becomes the dominant concern for null depth.

5.2 FREQUENCY CHANNELIZATION VS. TIME TAPS

Consider the rescue scenario shown in Figure 1 where $K = 10$ sensors are spaced over a one kilometer region. In order to locate signals 20 dB below the highest power signal, the bandwidth

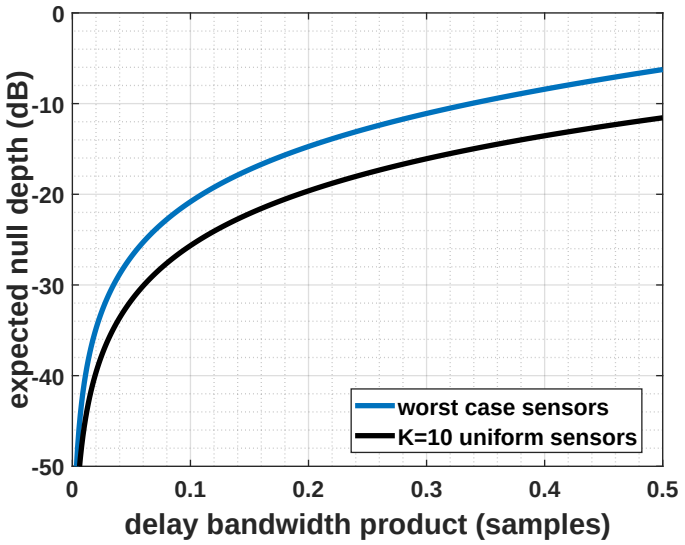

Figure 5. Expected null depth based on eigenvalue ratio for worst case of two sensor groups, and case of $K = 10$ sensors spread so that the delay spread is uniform.

that could be treated as narrowband is $b = 60$ kHz, using the nulldepth characterization in Figure 5. For a signal of analog bandwidth 1 MHz sampled at 2 MSamples/sec (MSps), this implies discrete-time processing using $N > 32$ frequency channels. Alternatively, the frequency channelization may be substituted with N time taps based on the alternation theorem for filter design.

For Doppler, consider a typical speed of 10 m/s for the UAVs, and a carrier frequency of 1 GHz. Assume that a burst of 1 ms is to be coherently integrated. Since the delay bandwidth product of 1/5 is much larger than the time Doppler product of 1/30, the effect of delay spread dominates. However, for a 6 ms burst, both delay spread and Doppler have equal effect.

Both the frequency channelization architecture, and the time taps architecture have been used to address signals that are wideband in the sense of delay bandwidth product for desired null depths. Figure 6 shows both architectures for the problem of beamforming, where the KN optimal complex weights $\mathbf{w}$ are used to combine the samples from the sensors and over time taps or frequency taps.

To make the discussion in this section more concrete, consider the least-squares [3] problem of determining STAP weights to recover the known signal samples $\mathbf{s}_{\text{pre}}$ (e.g., a preamble or template) from the measurement matrix $\mathbf{Z}$, $(K \times L)$

$$\mathbf{w}^{\text{opt}} = \arg\min_{\mathbf{w}} \left\| \mathbf{w}^H \mathbf{Z} - \mathbf{s}_{\text{pre}} \right\|^2 = \left(\mathbf{Z}\mathbf{Z}^H \right)^{-1} \mathbf{Z}\mathbf{s}_{\text{pre}}^H \tag{84}$$

where the computation of the weights involves inversion of the $K \times K$ covariance matrix $\mathbf{Z}\mathbf{Z}^H$, and $\mathbf{Z}\mathbf{s}_{\text{pre}}^H$ is an estimate of the amplitude and phase reponse of signal across the sensors. The sample

[3] often used synonymously with minimum mean squared error (MMSE) beamforming

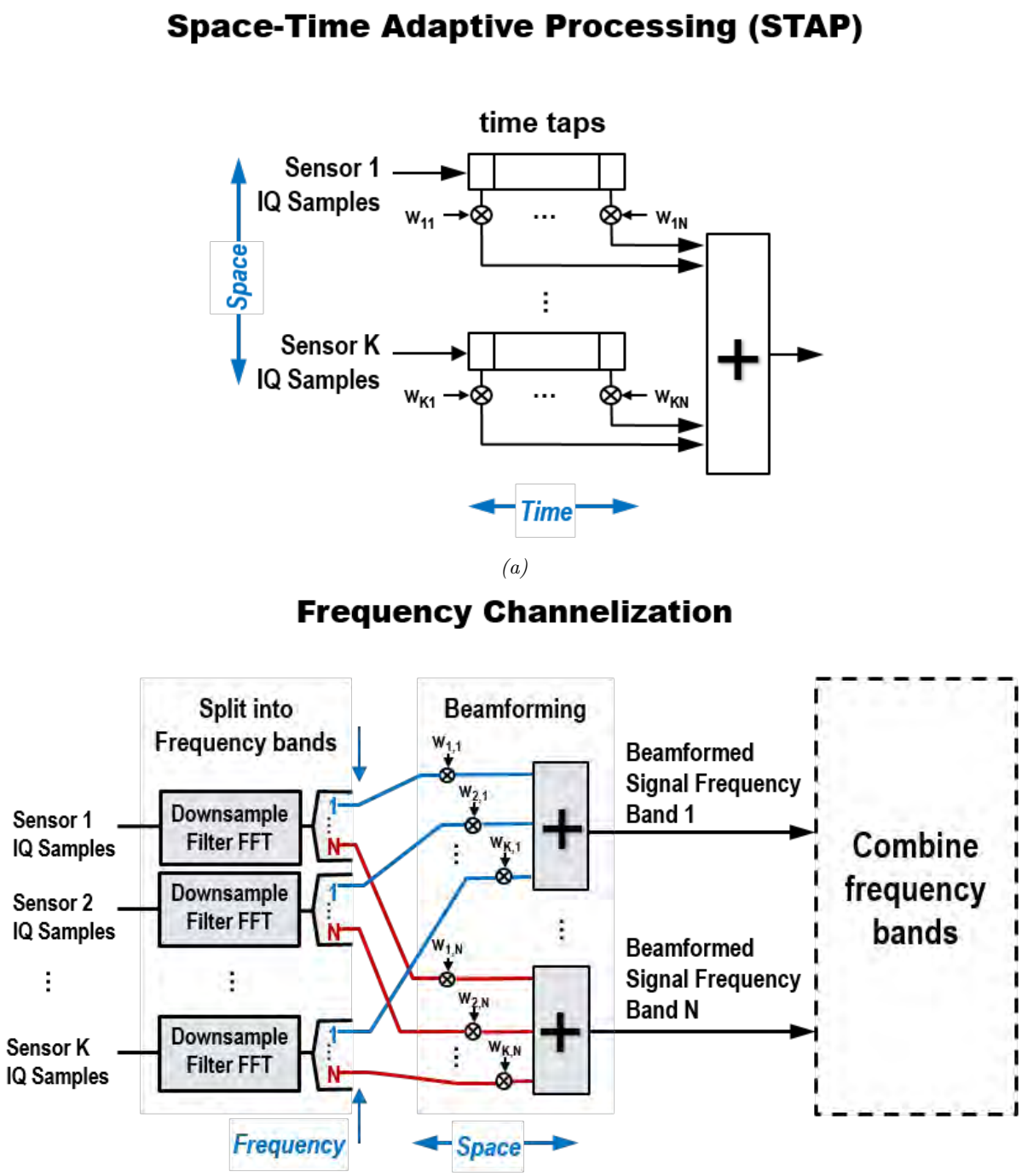

Figure 6. (a) architecture using time taps known as Space-Time Adaptive Processing (STAP). (b) architecture using frequency channelization. While the STAP architecture looks simpler in terms of applying the weights, computation of the weights involves matrix decomposition that is more computationally efficient in the frequency channelization architecture.

covariance $\mathbf{Z}\mathbf{Z}^H$ estimate improves with the number of samples, and $L > 3 * K$ is a rule of thumb for low signal-to-interference ratio loss [20], [21, Ch.9].

Based on the preceeding null depth discussion, the performance of the beamforming can be improved for wideband signals through time taps or frequency channelization. In the time taps setting, the beamforming problem of interest includes delayed versions of the measurements in the minimization, but the form of the solution remains the same

$$\widetilde{\mathbf{Z}} = \begin{bmatrix} \mathbf{Z} \\ \Delta^1\mathbf{Z} \\ \Delta^2\mathbf{Z} \\ \vdots \\ \Delta^N\mathbf{Z} \end{bmatrix} \tag{85}$$

where Δ^δ is a delay of δ applied to the measurements from each sensor (rows of $\mathbf{Z}$). The uniform sample delays of $\delta = (1, 2, \ldots, N)$ allow for a N time taps filter $\mathbf{w}(n)$ to account for delay spread. Adding the delayed samples then requires a $KN \times KN$ matrix inverse, along with sufficient time samples (both reference waveform and measured) to estimate the entries of the larger covariance matrix.

Alternatively, in a frequency channezilation architecture, the weights are obtained for each frequency by channelizing both the template and the measurements. At first glance, the sample requirement for covariance estimation in each frequency appears to be larger due to (1) the channelization filters, as the first channelization-filter-delay samples do not contribute (2) lower SNR in each frequency (3) no beneficial effect from $1/N$ reduction in the size of the covariance matrix, since the sample rate is downsampled by the same amount. However, it was observed empirically that the time taps architecture generally needed more samples in order to perform the same level of beamfofrming as the frequency channelized architecture. A possible reason for the discrepancy is shown in Figure 7. The correlation between frequency channels, i.e., the cross terms, is not computed in the frequency channelization approach; whereas, the STAP time taps architecture implicity computes all of the cross correlations.

5.2.1 Computational Complexity

In the STAP time taps architecture, the weights $\mathbf{w}$ are typically computed by QR decomposition of a $KN \times L$ matrix of samples requiring on the order of $(KN)^2$ multiples per step for L steps, where L is the integration time during which signals are expected to be stationary. On the other hand, computing the L independent QR decompositions of the $K \times L$ matrix for each frequency requires K^2N multiplies per step for L steps. The computational complexity is reduced by $1/N$, allowing the frequency-channelization approach to scale for larger delay spreads.

One way to improve the performance of the time taps architecture is to exploit the redundancy in the symmetric block-Toeplitz structure of the STAP covariance matrix. Let the data matrix $\mathbf{Z}$ be

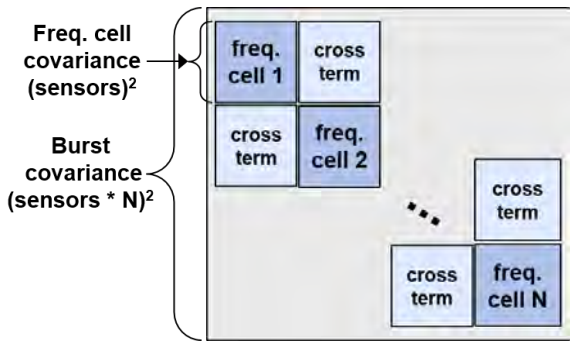

Figure 7. Structure in the covariance matrix of the samples from the perspective of frequency channelization. The naive STAP time taps architecture computes all elements of the matrix; whereas, the frequency-channelized architecture assumes that the cross terms are zero.

appended with zero columns so that integer sample delays can be expressed as a matrix operation.

$$\mathbf{Z} \leftarrow \begin{bmatrix} \mathbf{Z} & \mathbf{0}_{K\times 1} & \dots & \mathbf{0}_{K\times 1} \end{bmatrix} \tag{86}$$

$$\widetilde{\mathbf{Z}} = \begin{bmatrix} \mathbf{Z} \\ \mathbf{Z}\mathbf{S} \\ \mathbf{Z}\mathbf{S}^2 \\ \vdots \\ \mathbf{Z}\mathbf{S}^N \end{bmatrix} \tag{87}$$

where $\mathbf{S}$ is the delay by one sample shift matrix

$$\mathbf{S} = \begin{bmatrix} 0 & 1 & 0 & \dots & 0 \\ 0 & 0 & 1 & \dots & 0 \\ & & & \ddots & \\ 0 & 0 & 0 & \dots & 1 \\ 1 & 0 & 0 & \dots & 0 \end{bmatrix} \tag{88}$$

Then, the covariance matrix of time lags can be expressed as

$$\widetilde{\mathbf{Z}}\widetilde{\mathbf{Z}}^H = \left[\begin{array}{c|cccc} \mathbf{Z}\mathbf{Z}^H & \mathbf{Z}\left(\mathbf{S}^H\right)\mathbf{Z}^H & \mathbf{Z}\left(\mathbf{S}^H\right)^2\mathbf{Z}^H & \dots & \mathbf{Z}\left(\mathbf{S}^H\right)^N\mathbf{Z}^H \\ \mathbf{Z}\left(\mathbf{S}\right)\mathbf{Z}^H & \mathbf{Z}\mathbf{Z}^H & \mathbf{Z}\left(\mathbf{S}^H\right)\mathbf{Z}^H & \dots & \mathbf{Z}\left(\mathbf{S}^H\right)^{N-1}\mathbf{Z}^H \\ \mathbf{Z}\left(\mathbf{S}\right)^2\mathbf{Z}^H & \mathbf{Z}\left(\mathbf{S}\right)\mathbf{Z}^H & \mathbf{Z}\mathbf{Z}^H & \dots & \mathbf{Z}\left(\mathbf{S}^H\right)^{N-2}\mathbf{Z}^H \\ \vdots & \vdots & \vdots & \ddots & \vdots \\ \mathbf{Z}\left(\mathbf{S}\right)^N\mathbf{Z}^H & \mathbf{Z}\left(\mathbf{S}\right)^{N-1}\mathbf{Z}^H & \mathbf{Z}\left(\mathbf{S}\right)^{N-2}\mathbf{Z}^H & \dots & \mathbf{Z}\mathbf{Z}^H \end{array}\right] \tag{89}$$

where the Toeplitz block symmetric structure is observed, and all block entries are related to the first row or column. A Levinson inversion algorithm could then be used to efficiently determine the matrix inverse. However, such an approach operates in the power domain and encounters the issue

of doubling bit depth. Redundancy could also be exploited in the time domain avoiding the issue of bit depth [22], [23, Chapter 7], but this approach is not simple to understand. Furthermore, using the structure of the covariance can lead to gains in performance, as shown in [24] for the AEP detector.

5.2.2 Filter Bank Design

Finite-impulse response (FIR) filter banks, often obtained from frequency modulating a prototype baseband FIR filter $h(n)$ to a passband, may be used to break up a wideband signal into frequency components (a process called analysis) and stitch back frequency components to produce a wideband copy (a process called synthesis). The received signals from each of the sensors passes through a separate analysis filter bank. Adaptive beamforming of the narrowband signals is then performed, and the result is synthesized to allow for waveform recovery and bit decisions.

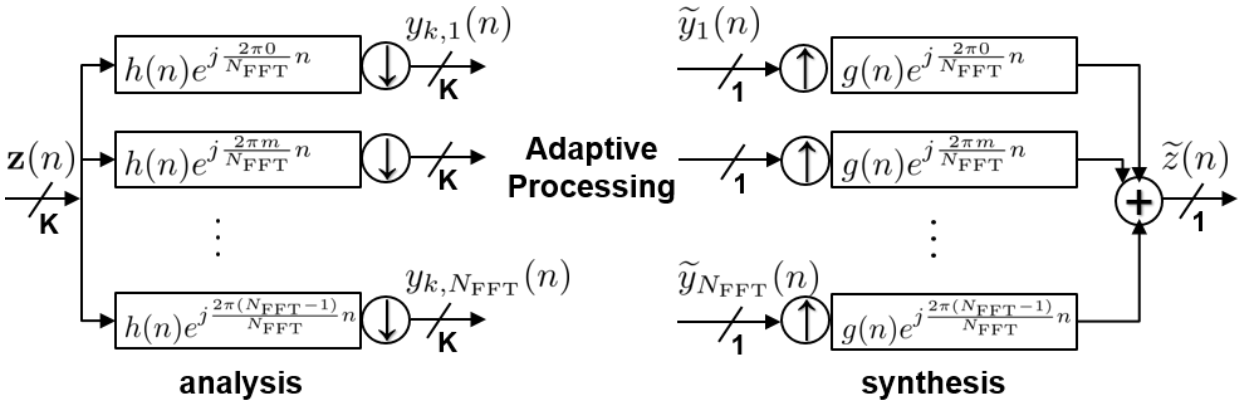

Figure 8. Block diagram of analysis $h(n)$ and synthesis $g(n)$ filter bank for adaptive processing of K sensors. N_{FFT} channels are adaptively processed at a downsampled rate and interpolated to create a single output stream. Here each branch corresponds to a different frequency band, whereas in Figure 6b, each branch is a different sensor. However, both figures are depicting a frequency channelized architecture.

Several approaches to design of the analysis and synthesis filter banks were considered and evaluated for reconstruction error. The design parameters included the length of the filters, the oversampling rate (multiplier on the critical downsampling of $1/N_{\mathrm{FFT}}$), and the number of frequency channels N_{FFT}. The equivalent polyphase implementation of the processing in Figure 8 is shown in Figure 9.

For the chosen quadrature mirror filters (QMF) approach [25], the analysis and synthesis filters are the same up to a phase. The filter design approach considered was originally designed for cosine-modulated filter banks, but shown to be a form of complex-exponential modulation [26, Eqn.2,Appendix]. The baseband filter $h(n) = g(n)$ is modulated as

$$h_m(n) = h(n)e^{j\frac{2\pi m}{N_{\mathrm{FFT}}}n} \tag{90}$$

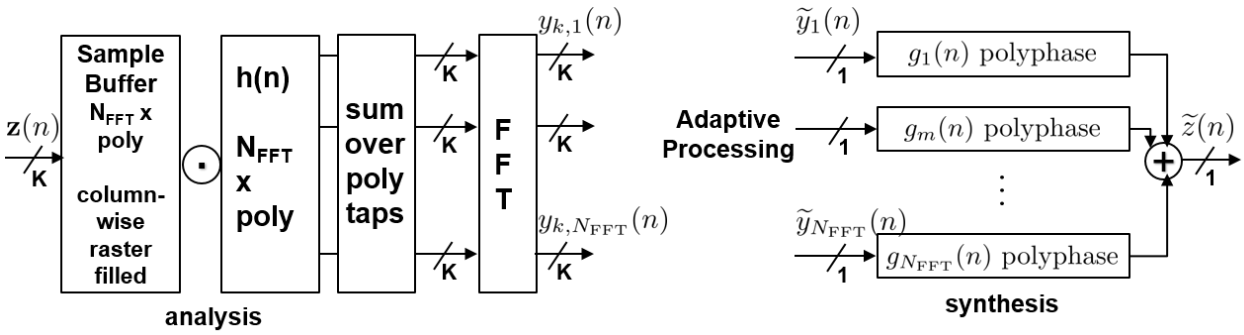

Figure 9. Polyphase implementation of analysis $h(n)$ and synthesis $g(n)$ filter bank for adaptive processing of K sensors. Downsampling achieved by shifting samples in the sample buffer forward by N_{FFT}/oversampling rate. Analysis filter is reshaped into a ($N_{FFT} \times$ polyphase taps) matrix and dot multiplied with the sample buffer and added, before taking an FFT.

The filter design optimization starts with $h(n)$ initialized as a Parks-McClellan equiripple FIR filter, and iteratively minimizes the reconstruction error through a quadratic minimization with linear constraints [25, Eqn. 40].

The residual error from analysis and synthesis of a BPSK signal (802.11b 11-chip Barker spread BPSK was used as an example) is shown in Figure 10. The residual is defined as the least-squares error between the original signal and the reconstructed signal. Based on the desired residuals below 30 dB, an oversampling rate of 2 was selected. Figure 11 shows the impulse response for a $N_{\mathrm{FFT}} = 16$ band prototype filter $h(n)$ with 4 polyphase taps.

5.3 FREQUENCY CHANNELIZATION NOTATION

Define the output of each passband filter as $y_{k,m}(n)$ where m is the frequency index, k is the sensor index, and n is the sample index.

$$y_{k,m}(n) = (h_m \circledast z_k)\left(\frac{N_{\mathrm{FFT}}}{2} \cdot n\right) \tag{91}$$

where $\circledast$ represents convolution, and the result is downsampled by $\frac{N_{\mathrm{FFT}}}{2}$ in the time index for the chosen oversampling rate of 2. Convolution with the filter produces samples at the passband, which are effectively shifted to complex baseband through the downsampling operation. There is typically a demodulation term $e^{j\pi k(n-1)}$ that evaluates to a spectrum flip for odd k, but is not needed due to multiplying by the conjugate modulation term for reconstruction. In the same way as for the wideband samples, define the data matrix of samples over time for a particular frequency as

$$\mathbf{Y}_m = \begin{bmatrix} y_{1,m}(0) & y_{1,m}(1) & \dots & y_{1,m}(\bar{L}) \\ y_{2,m}(0) & y_{2,m}(1) & \dots & y_{2,m}(\bar{L}) \\ \vdots & & & \\ y_{K,m}(0) & y_{K,m}(1) & \dots & y_{K,m}(\bar{L}) \end{bmatrix} \tag{92}$$

where $\bar{L}$ is the number of samples at the downsampled rate (compared to L samples at the wideband sample rate). Note that the frequency channelization (and similarly reconstruction) introduce a sample delay, which for the proposed filters is the number of polyphase taps. It is important to account for these delays when considering the demod/remod approach to be presented.

It is convenient to refer to the collection of matrices over all frequencies as

$$\mathbf{Y} = \{\mathbf{Y}_1, \mathbf{Y}_2, \ldots, \mathbf{Y}_{N_{\mathrm{FFT}}}\} \tag{93}$$

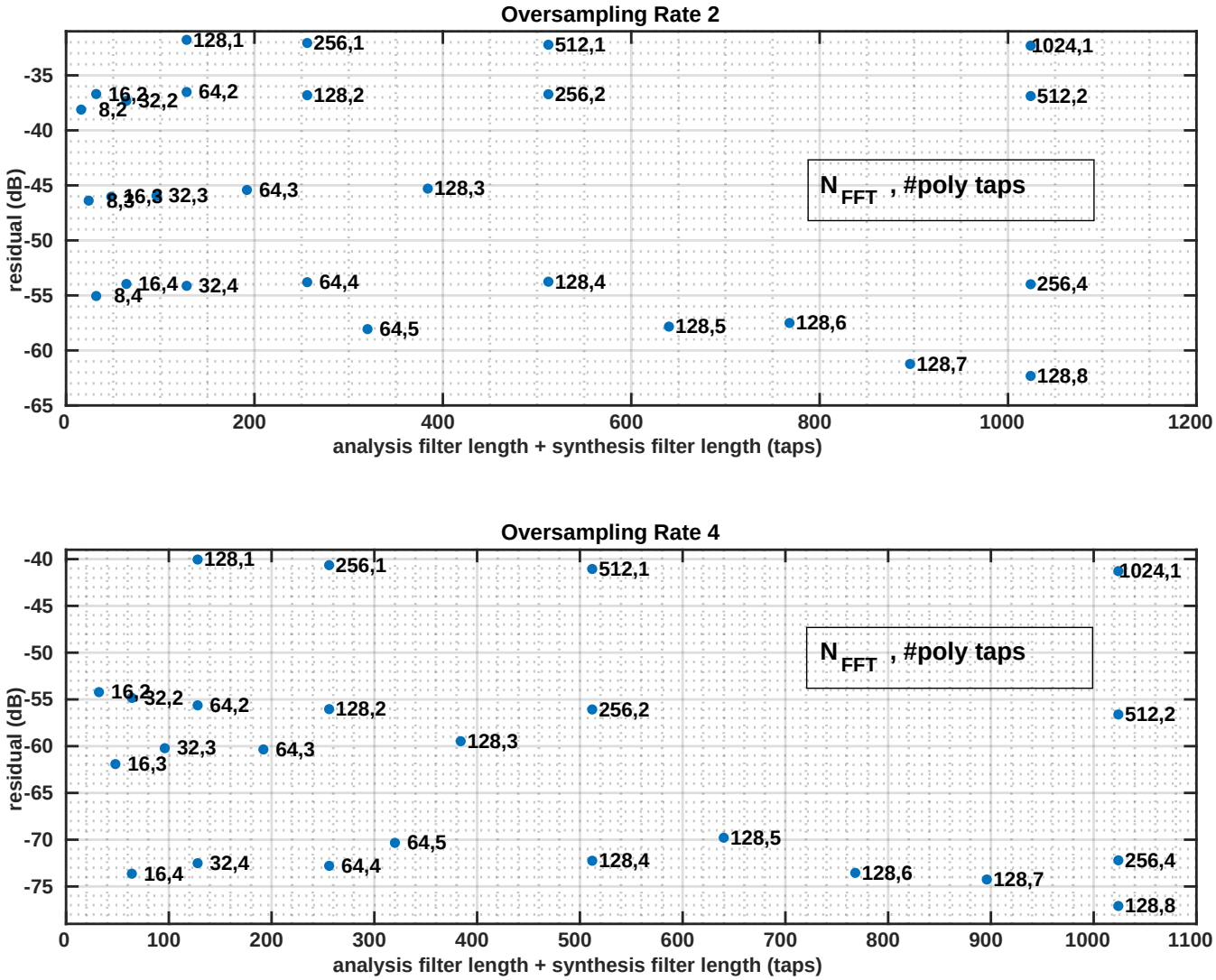

*Figure 10. Residual from signal analysis and synthesis of a spread BPSK signal using number of frequency channels N_{FFT}, polyphase taps as indicated, and either oversampling by 2 (i.e. downsampling of $\frac{N_{FFT}}{2}$) or oversampling by 4. The analysis and synthesis filters are the same for these QMF designs, and the total number of taps is $N_{FFT} * $ polyphase taps.*

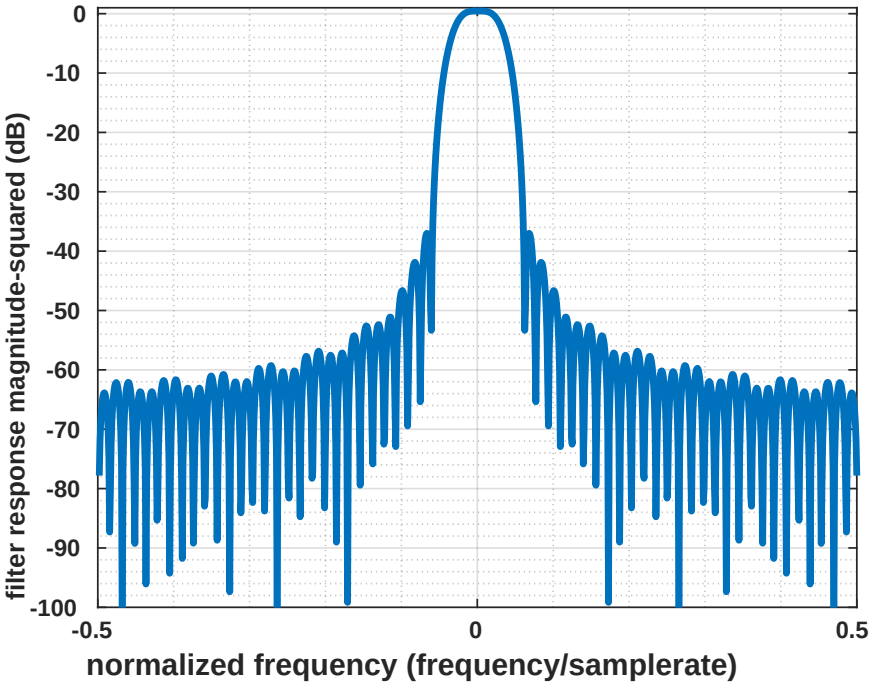

Figure 11. Designed prototype filter for $N = 16$ frequency channels that uses 4 polyphase taps to achieve -55 dB residual error (see Figure 10) in the reconstruction for an oversampling rate of 2.

6. WIDEBAND AEP

Compared to adaptive detection using a template matched filter (e.g. via the least-squares metric (84)), adaptive event processing (AEP) detection techniques can offer computational benefits since a search over frequency offsets between sensors and for the source center frequency can be avoided [4]. The AEP approach to detection and geolocation can be developed for the wideband context by starting with the narrowband detection problem, where the signal model is [3].

$$\mathbf{Z} = \mathbf{XAT} + \mathbf{N} \tag{94}$$

where $\mathbf{X}$ is the $K \times J$ matrix of sensor responses, $\mathbf{A}$ is the $J \times S$ matrix of symbols, $\mathbf{T}$ is the $S \times L$ matrix of time samples, and $\mathbf{N}$ is complex additive white Gaussian noise. For change detection, the unknown signal turn on is modeled as

$$\begin{array}{rcl} \mathbf{T} & = & \begin{bmatrix} 0 & \ldots & 0 & 1 & \ldots & 1 \end{bmatrix} \\ \mathbf{Z} & = & \begin{bmatrix} \underbrace{\mathbf{Z}_q}_{\text{old looks}} & & \underbrace{\mathbf{Z}_p}_{\text{new looks}} \end{bmatrix} \end{array} \tag{95}$$

where the observations are partitioned into old looks $\mathbf{Z}_q$ (where an unknown signal is absent) and new looks $\mathbf{Z}_p$ (where the unknown signal is present). Note that the unknown waveform samples are modeled by $\mathbf{A}$ in this case.

The corresponding generalized likelihood ratio test (GLRT) [27], [3, Eqn.8] can be shown to be a ratio of determinants maximized over the unknown signal response vectors [5].

$$\text{GLRT}\left(\mathbf{Z}, \mathbf{T}\right) = \max_{\mathbf{X}} \left(\frac{\left| \mathbf{X}^H \left(\mathbf{Z}_q \mathbf{Z}_q^H \right)^{-1} \mathbf{X} \right|}{\left| \mathbf{X}^H \left(\mathbf{Z}\mathbf{Z}^H \right)^{-1} \mathbf{X} \right|} \right)^L \tag{96}$$

When there is a single new signal, $J = 1$, $\mathbf{X}$ is a vector and the determinants becomes scalars. This leads to the eigenvalue solution

$$\text{GLRT}\left(\mathbf{Z}, \mathbf{T}\right) = \lambda_{\max} \left\{ \left(\mathbf{Z}\mathbf{Z}^H \right) \left(\mathbf{Z}_q \mathbf{Z}_q^H \right)^{-1} \right\} = 1 + \lambda_{\max} \left\{ \left(\mathbf{Z}_p \mathbf{Z}_p^H \right) \left(\mathbf{Z}_q \mathbf{Z}_q^H \right)^{-1} \right\} \tag{97}$$

where the argument $\{\cdot\}$ is a contrast matrix or whitened covariance matrix. The corresponding estimate of the response vector $\mathbf{X}$ from the eigenvalue solution is

$$\mathbf{X} = \mathbf{e}_{\max} \left\{ \left(\mathbf{Z}\mathbf{Z}^H \right) \left(\mathbf{Z}_q \mathbf{Z}_q^H \right)^{-1} \right\} = \mathbf{e}_{\max} \left\{ \left(\mathbf{Z}_p \mathbf{Z}_p^H \right) \left(\mathbf{Z}_q \mathbf{Z}_q^H \right)^{-1} \right\} \tag{98}$$

Implementation of the AEP approach may involve diagonal loading to account for ill-conditioning in the covariance matrices. Trace is commonly used as a computationally efficient approximation of the max eigenvalue.

[4] A comparison of these techniques in terms of performance is not presented here.

[5] The dependency on $\mathbf{A}$, and on the covariance of the noise $\mathbb{E}\left\{\mathbf{N}\mathbf{N}^H\right\}$ in the numerator and denominator of original maximum likelihood expression is eliminated due to the maximization over these unknown parameters, which leads to the generalization of the ML detector.

Using the frequency-channelized architecture to break up the wideband detection problem into N independent narrowband components, the wideband detection statistic becomes a product of likelihoods (see notation in Section 5.3)

$$\boxed{\text{Wideband GLRT}\left(\mathbf{Y},\mathbf{T}\right)=\prod_{m=1}^{N}\left(1+\lambda_{\max}\left\{\mathbf{R}_{p,m}\mathbf{R}_{q,m}^{-1}\right\}\right)} \tag{99}$$

where $\mathbf{R}_{p,m}=\mathbf{Y}_{p,m}\mathbf{Y}_{p,m}^{H}$ (similarly $\mathbf{R}_{q,m}$) is the covariance matrix of the channelized measurements in the m-th band, and the corresponding response vectors can be collected into a $K\times N$ matrix

$$\mathbf{V}=\left[\begin{array}{cccc}| & | & & | \\ \mathbf{X}_1 & \mathbf{X}_2 & \ldots & \mathbf{X}_N \\ | & | & & |\end{array}\right] \tag{100}$$

6.1 GEOLOCATION

An experimentally validated approach for geolocation is to obtain time correlation estimates using just the phase differences between response vectors, which should vary linearly over frequency according to the channel model (44). The correlation estimate between sensors k and l at time lag τ is

$$\rho_{k,l}(\tau)=\sum_{m=1}^{N}\frac{\mathbf{V}_{k,m}\mathbf{V}_{l,m}^{*}}{\left|\mathbf{V}_{k,m}\right|\left|\mathbf{V}_{l,m}\right|}\,e^{j\omega_m\tau} \tag{101}$$

where $\mathbf{V}_{k,m}$ is the k-th sensor and m-th frequency channel, and ω_m is the channelized center frequency. The operation can be implemented using an inverse-FFT (IFFT) for sample delays and uniformly-spaced frequency channelization. The effect of the normalization in the denominator is to remove the channel gain (which is constant over frequency) but primarily to account for any frequency varying effects due to whitening. For time estimates, such phase only techniques, called Phase Transform (PHAT), have been suggested along with other GCC techniques to deal with waveform irregularities [17].

Once the pairwise cross correlations have been computed, resistive combining can then be used to produce a geolocation image. The performance of the geolocation depends on the ability to estimate delays using the N response vectors that sample the receive bandwidth. Section 5.1 discussed the issue of eigenvalue spread in each frequency, which is one issue that determines the choice of N. A more basic requirement is that the number of frequency channels needs to larger than the delay spread in samples for any pair of sensors for the signal of interest. This is just a sampling requirement in frequency in order to estimate delay.

6.2 ADJACENT FREQUENCIES

One way to include the effect of adjacent frequencies in the detection statistic and response vector estimate is to form the GLRT (96) using $m-1, m, m+1$ frequency channels [6], but restrict the response vector $\mathbf{X}$ to have zeros in the neighboring $m-1, m+1$ components. Define the appended measurements

$$\widetilde{\mathbf{Y}}_q = \begin{bmatrix} \mathbf{Y}_{q,m-1} \\ \mathbf{Y}_{q,m} \\ \mathbf{Y}_{q,m+1} \end{bmatrix} \tag{102}$$

and form $\boldsymbol{\Upsilon}_q = (\widetilde{\mathbf{Y}}_q \widetilde{\mathbf{Y}}_q^H)^{-1}$ for the numerator, and similarly $\boldsymbol{\Upsilon} = (\widetilde{\mathbf{Y}}\widetilde{\mathbf{Y}}^H)^{-1}$ for the denominator in the GLRT expression. The GLRT statistic can then be formed by taking the central portion of the inverses corresponding to the m-th frequency,

$$\text{GLRT adjacent}\,(\mathbf{Y}, \mathbf{T}) = \lambda_{\max}\left\{ \left([\boldsymbol{\Upsilon}]_{(m,m)} \right)^{-1} [\boldsymbol{\Upsilon}_q]_{(m,m)} \right\} \tag{103}$$

where the operator $[\,\cdot\,]_{(m,m)}$ picks the $K \times K$ central matrix of the $3K \times 3K$ matrix containing the $m-1, m, m+1$ adjacent frequencies. Such an approach allows for detection and response vector estimation using fewer samples and may help with Doppler.

[6] The number of neighbors could be more depending on the expected correlation between frequencies present in the waveform and due to the channel.

This page intentionally left blank.

7. WIDEBAND MUSIC

In the narrowband context, the multiple signal classification (MUSIC) problem [28] is to recover the sensor response(s) and corresponding direction of arrival(s) (DOAs) of source(s) simultaneously present in the estimated spatial covariance modeled as

$$\mathbf{R}_m = \mathbf{Y}_m \mathbf{Y}_m^H = \mathbf{V}_m \mathbf{P}_m \mathbf{V}_m^H + \sigma_m^2 \mathbf{I} \tag{104}$$

where m is the index for the frequency channel, $\mathbf{V}_m$ is the $K \times S$ matrix of sensor responses for S sources, $\mathbf{P}_m$ is a $S \times S$ diagonal matrix of source powers, and σ_m^2 is the noise variance.

When the number of sources is known, the covariance can be decomposed into signal and noise subspaces through eigenvalue decomposition

$$\mathbf{R}_m = \mathbf{E}_{\mathrm{s},m} \mathbf{\Lambda}_{\mathrm{s},m} \mathbf{E}_{\mathrm{s},m}^H + \mathbf{E}_{\mathrm{n},m} \mathbf{\Lambda}_{\mathrm{n},m} \mathbf{E}_{\mathrm{n},m}^H \tag{105}$$

where $\mathbf{E}_{\mathrm{s},m}$ is the $K \times S$ matrix of signal eigenvectors with corresponding eigenvalues on the diagonals of $\mathbf{\Lambda}_{\mathrm{s},m}$ and similarly for the noise subspace. Assuming that the eigenvalues in the noise subspace are all approximately the same

$$\mathbf{R}_m = \mathbf{E}_{\mathrm{s},m} \left(\mathbf{\Lambda}_{\mathrm{s},m} - \gamma \mathbf{I} \right) \mathbf{E}_{\mathrm{s},m}^H + \gamma \mathbf{I} \tag{106}$$

Traditionally, the largest gap in the eigenvalues is assumed to separate the signal and noise eigenvalues (and corresponding eigenvectors), and γ is estimated as the average of the bottom $K - S$ eigenvalues.

The MUSIC metric is the distance between the modeled narrowband sensor response vector and the estimated signal subspace

$$\begin{aligned} \Phi_m(\mathbf{x}_0) &= \left\| \mathbf{v}_m(\mathbf{x}_0)^H \mathbf{E}_{\mathrm{s},m} \right\|^2 \\ &= \mathbf{v}_m(\mathbf{x}_0)^H \mathbf{E}_{\mathrm{s},m} \mathbf{E}_{\mathrm{s},m}^H \mathbf{v}_m(\mathbf{x}_0) \end{aligned} \tag{107}$$

where $\mathbf{v}_m = e^{j\omega_m \boldsymbol{\tau}(\mathbf{x_0})}$.

For the gain and delay model (44), a metric for consideration is to average the narrowband metric over frequency, maximizing over the unknown complex gains $\mathbf{g}$

$$\Phi(\mathbf{x}_0) = \max_{\|\mathbf{g}\|=1} \frac{1}{N} \sum_{m=1}^{N} \left(\mathbf{v}_m \odot \mathbf{g} \right)^H \mathbf{E}_{\mathrm{s},m} \mathbf{E}_{\mathrm{s},m}^H \left(\mathbf{v}_m \odot \mathbf{g} \right) \tag{108}$$

$$= \max_{\|\mathbf{g}\|=1} \frac{1}{N} \mathbf{g}^H \left[\sum_{m=1}^{N} \mathrm{diag}\left(\mathbf{v}_m \right)^H \mathbf{E}_{\mathrm{s},m} \mathbf{E}_{\mathrm{s},m}^H \mathrm{diag}\left(\mathbf{v}_m \right) \right] \mathbf{g} \tag{109}$$

where $\odot$ represents element-wise multiplication. In this form, maximizing over $\mathbf{g}$ is recognized as an eigenvalue problem with $\mathbf{g}$ as the largest eigenvector of the matrix in brackets, and the metric as the largest eigenvalue [5, Eqn.13-14]

$$\boxed{\Phi(\mathbf{x}_0) = \lambda_{\max} \left\{ \sum_{m=1}^{N} \mathrm{diag}\left(\mathbf{v}_m \right)^H \mathbf{E}_{\mathrm{s},m} \mathbf{E}_{\mathrm{s},m}^H \mathrm{diag}\left(\mathbf{v}_m \right) \right\}} \tag{110}$$

When the channel has differential Doppler shifts across the sensors, the MUSIC metric may be modified [7] [29] to account for the expected differential Dopplers at a given hypothesis position $\mathbf{x}_0$. This allows for the signal of interest to be focused but causes any other signals present to be unfocused, leading to eigenvalue spread in each frequency channel, and poor resolution in the metric. When Doppler is present, methods other than eigenvalue gap may be needed to identify subspaces that are useful to the overall metric.

[7] Applying the differential Doppler for each position before frequency channelization requires more computation compared to applying the differential Doppler for each position after channelization and before eigenanalysis.

8. WIDEBAND DEMOD/REMOD

The frequency-channelized wideband beamforming approach including a demodulation and remodulation step has an implementation that is difficult to describe, and involves iteration. The approach starts with a known preamble $s_{\text{pre}}(n)$ that is frequency channelized, along with the wideband data to be demodulated.

$$s_{m,\text{pre}}(n) = (h_m \circledast s_{\text{pre}}) \left(\frac{N_{\text{FFT}}}{2} \cdot n \right) \tag{111}$$

The assumption is that a detection process (either matched filter or AEP) has already been performed to frequency and time shift the preamble waveform, and apply differential time and frequency shifts to the data to achieve the initial synchronization.

In each frequency, the beamforming weights are computed on the synchronized preamble and the adjusted data according to

$$\mathbf{w}_m^{\text{opt}} = \arg \min_{\mathbf{w}_m} \left\| \mathbf{w}_m^H \mathbf{Y}_m - \mathbf{s}_{m,\text{pre}} \right\|^2 = \left(\mathbf{Y}_m \mathbf{Y}_m^H \right)^{-1} \mathbf{Y}_m \mathbf{s}_{m,\text{pre}}^H \tag{112}$$

Over the entire bandwidth of the signal, the relative complex scaling of the weights recovers the wideband signal $s_{\text{pre}}(n)$. Whereas it is common to normalize the weights by setting the complex gain of an arbitrary reference sensor to one, no weight normalization is needed here due to the knowledge of the preamble.

In each frequency, the weights are applied to samples forward in time from the preamble to recover new (unknown) channelized symbols. The channelized symbols are reconstructed using the synthesis filter, so that symbol decisions can be made. Then, channelizing the symbol decisions provides an update to the preamble waveform in each frequency

$$s_{m,\text{pre}}(n) \leftarrow \left[\; s_{m,\text{pre}}(n) \quad \text{channelized symbol decisions} \; \right] \tag{113}$$

Over the course of the demod/remod iterations, careful attention has to be paid to the delay due to analysis and synthesis. Once the entire waveform has been recovered, the maximum likelihood techniques covered in Section 2 may then be used for geolocation.

This page intentionally left blank.

9. SIMULATIONS

In this section, two scenarios are presented, and a subset of the geolocation techniques is evaluated.

9.1 FOUR 802.11b SOURCES EXAMPLE

Consider the geometry and scenario shown in Figure 12 where ten sensors are in a 2 km box that contains four 802.11b sources transmitting (also called transmitters here) at different power levels, different start times and for different duration. The sensors are located 30 meters above a flat ground where the sources are located. The sensors are moving with random velocity components chosen with standard deviation of 10 m/s in the x, and y directions and zero z velocity.

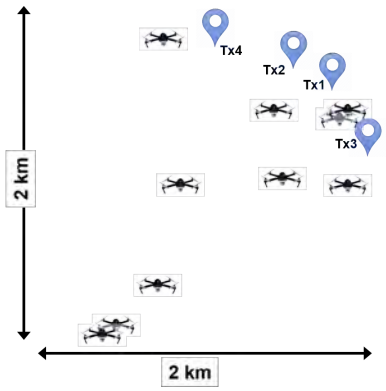

(a) Positions of four sources and ten sensors

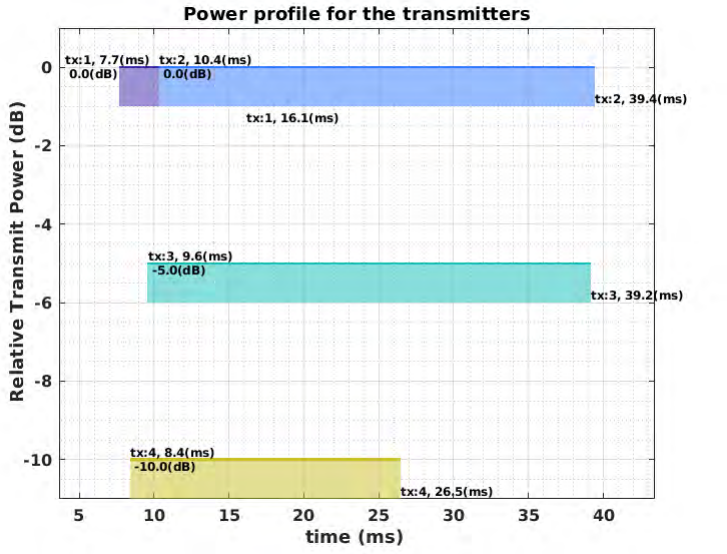

(b) Relative powers and duration of the sources

Figure 12. Geometry and setup of an example detection and geolocation problem for Wifi signals.

Figure 13 shows a comparison of the frequency-channelized AEP detector (103) with AEP detectors using time taps. The 415-tap AEP detector has uniform time taps, whereas the 4-tap AEP detector uses genie knowledge of the delays for the four signals to place sparse taps. The frequency channelized AEP detector using adjacent frequencies is able to detect transmitter 2, whereas the 415-tap AEP detector does not. Although the sparse taps approach is based on genie knowledge, this example shows the possible utility in using cross-correlation peaks to pick taps, particularly with signals of similar power and when only two signals are present.

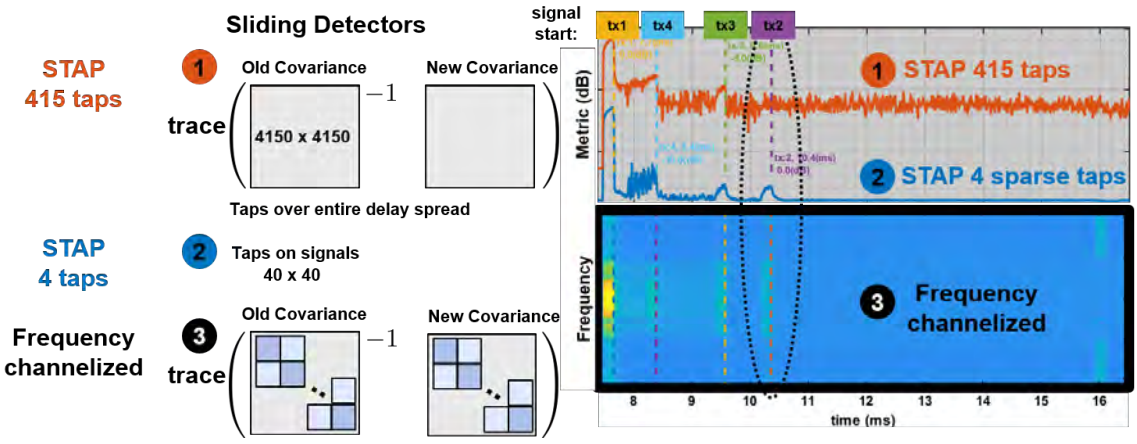

Figure 13. Comparison of time-taps AEP vs. sparse taps AEP vs. frequency-channelized AEP for detection of four 802.11b sources using a ten element sparse array. The dashed lines indicate the start of a burst, and the power of the user – either 0 dB,0 dB,-5 dB, or -10 dB. The 415 time-taps AEP = 4150 × 4150 covariance took two days to run using 12 processors, but achieves no better performance than using sparse taps placed at the known signal delays. The frequency-channelized AEP is able to pick up both the start and end of signals. The time-taps AEP is sample starved, since the covariance is developed using 4224 independent samples, whereas 3(10 sensors * 415 taps) is typically necessary for good beamforming performance.*

Figure 14 shows the cross-correlation resistive combining geolocation image when the signals have the same power compared to when the signals have different powers [0 dB,0 dB,-5 dB, -10 dB] corresponding to transmitters 1-4. The signal from transmitter 4 at 10 dB below the highest power signals from transmitters 1-2 is not located. Figure 15 shows the geolocation image obtained from using the correlation estimates from the AEP detection approach (101). Again, the -5 dB source is located, but the -10 dB source does not produce a large peak in the geolocation image. In the AEP approach, the detection also produces a time of arrival (and potentially an end time) that could help with signal copy or selecting intervals of the data to process.

For this example, the wideband MUSIC approach fails due to the presence of a large differential Doppler spread. Since the center frequency of the signal is 2.9 GHz, the computed spread of more than 100 Hz is too large for the signal duration of 8 to 30 ms.

The demod/remod approach was not implemented for the 802.11b signal. For the Barker-spread signal, such an approach involves despreading based on the preamble synchronization. However, even with moderate bit errors, a recovered waveform is able to locate the smallest source.

9.2 BALLOONS EXAMPLE

Consider the geometry and scenario shown in Figure 16 where ten high-altitude balloons, 30 km above ground level (AGL), are in a 100 km diameter circle that contains two 100 kHz bandwidth quadrature phase-shift keying (QPSK) sources on the ground transmitting at two power

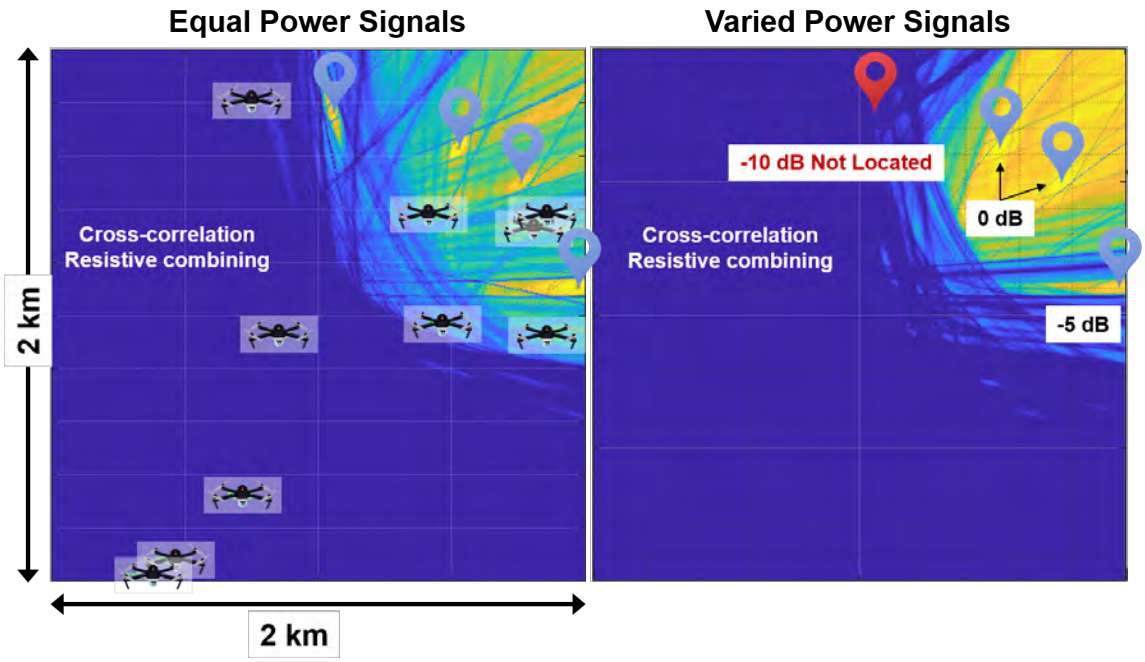

Figure 14. Comparison of cross-correlation resistive combining performance when the signal powers are the same vs. when the signal powers are 0 dB,0 dB,-5 dB, or -10 dB for transmitters 1-4, respectively.

levels, two different start times and for two different durations. The balloons are moving with random velocity components chosen with standard deviation of 10 m/s in the x, and y directions and zero z velocity. The ultra high frequency (UHF) signals have a center frequency of 300 MHz, and the transmit power for the higher power transmitter 1 is 100 mW.

Figure 17 shows a comparison of three geolocation approaches: cross-correlation resistive combining, MUSIC, and demod/remod. Whereas the cross-correlation approach has sidelobes from transmitter 1 above the level of transmitter 2, both the other beamforming approaches are able to locate transmitter 2, which is 10 dB lower in power. The advantage of the demod/remod approach is that it recovers the QPSK symbols, which can be used for verification, with 9% bit errors, in this example. Since the center frequency of the signal is 300 MHz, the Doppler spread is not significant for the signal duration.

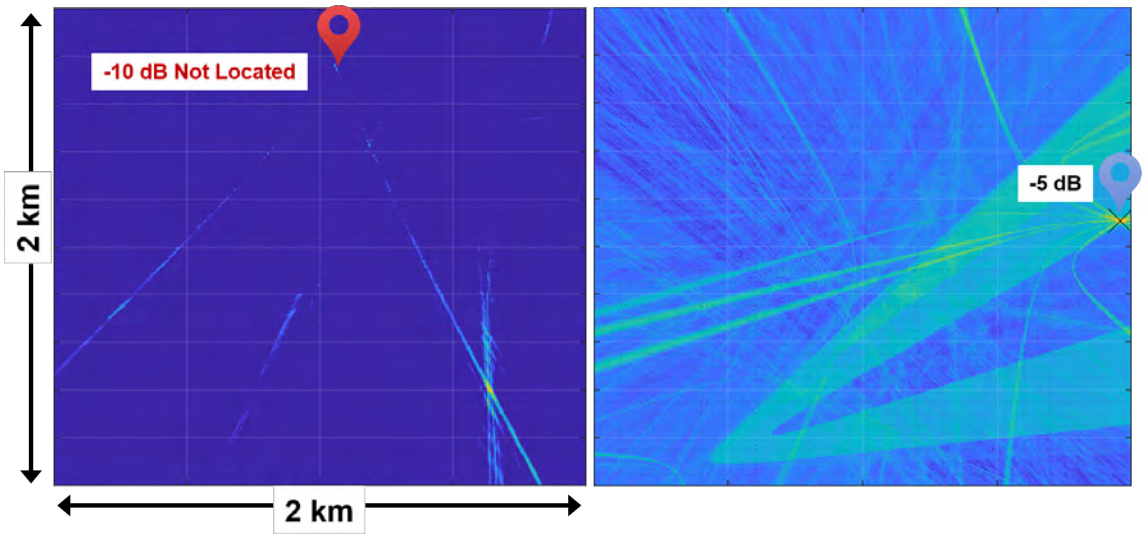

Figure 15. Correlation estimates from frequency-channelized AEP used to produce a resistively combined geolocation image. The -10 dB power signal does not have a strong peak, but the -5 dB power signal is located.

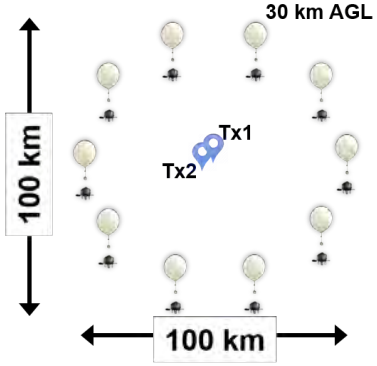

(a) Positions of two sources and ten sensors

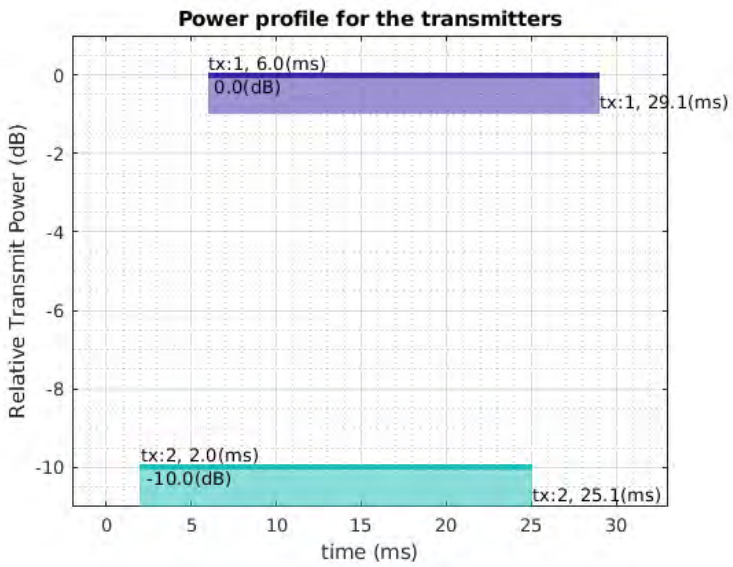

(b) Relative powers and duration of the sources

Figure 16. Geometry and setup of an example detection and geolocation problem involving balloons at 30 km above the ground.

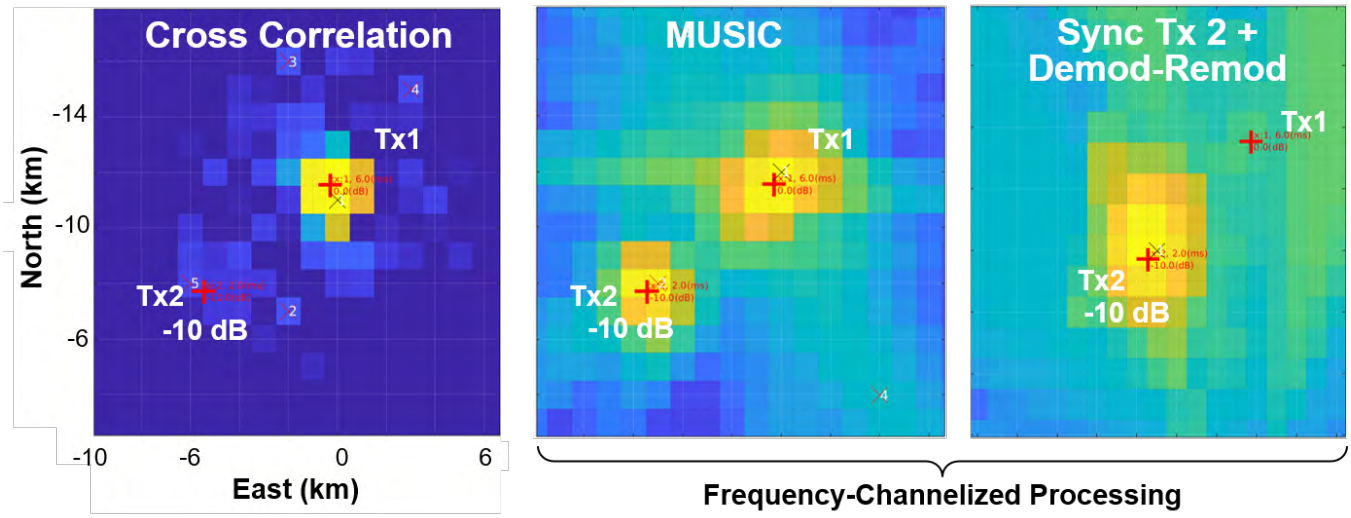

Figure 17. Comparison of three geolocation approaches for a balloon scenario, where cross-correlation fails, but the beamforming approaches are successful.

This page intentionally left blank.

10. CONCLUSION

The topic of gelocation in the presence of interference has been introduced, and several beamforming approaches have been described. Implementation of these approaches and application to simulated data shows their utility. Although the focus of the treatment here has been on TDOA, some of the approaches extend to frequency difference of arrival (FDOA). Detailed analysis of the performance of the approaches and their applicability in different operating regimes requires further study.

This page intentionally left blank.

A QUADRATIC EQUATION FOR TIME DELAY

Squaring both sides of the delay equation (3), a quadratic equation can be obtained for $c\tau$ when linear motion is considered

$$\begin{aligned} c^2\,\tau(t)^2 &= \|\mathbf{x}_k(t) - \mathbf{x}_0(t+\tau(t))\|^2 \\ &= \|(\mathbf{v}_k \cdot t + \mathbf{x}_k) - (\mathbf{v}_0 \cdot (t+\tau) + \mathbf{x}_0)\|^2 \\ &= \left\| \underbrace{(\mathbf{v}_k - \mathbf{v}_0)}_{\mathbf{v}_d} \cdot t + \mathbf{v}_0 \cdot \tau + \underbrace{(\mathbf{x}_k - \mathbf{x}_0)}_{\mathbf{x}_d} \right\|^2 \\ 0 &= \underbrace{\left(|\mathbf{v}_0|^2 - c^2\right)}_{a_2}\tau^2 + \underbrace{2\left(\mathbf{v}_d^T\mathbf{v}_0 t + \mathbf{v}_0^T\mathbf{x}_d\right)}_{a_1}\tau + \underbrace{2\mathbf{v}_d^T\mathbf{x}_d t + |\mathbf{x}_d|^2 + |\mathbf{v}_d|^2\,t^2}_{a_0} \end{aligned} \tag{A.114}$$

where $\mathbf{x}_k = \mathbf{x}_k(t=0)$ is the position of the platform at time zero, similarly $\mathbf{x}_0 = \mathbf{x}_0(t=0)$, and $\mathbf{x}_d \triangleq \mathbf{x}_k - \mathbf{x}_0$, similarly $\mathbf{v}_d \triangleq \mathbf{v}_k - \mathbf{v}_0$ represent the differences in position and velocity. The two solutions are obtained from the quadratic formula as $\tau^* = (2a_2)^{-1}\left(-a_1 \pm \sqrt{a_1^2 - 4\,a_2\,a_0}\right)$

This page intentionally left blank.

GLOSSARY

AEP	Adaptive Event Processing
BPSK	Binary Phase Shift Keying
CAF	Cross Ambiguity Function
DOA	Direction of Arrival
DPD	Direct Position Determination
FDOA	Frequency Difference of Arrival
FIR	Finite Impulse Response
FFT	Fast Fourier Transform
GCC	Generalized Cross Correlation
GLRT	Generalized Likelihood Ratio Test
GPS	Global Positioning System
IFFT	Inverse Fast Fourier Transform
LL	Lincoln Laboratory
MIT	Massachusetts Institute of Technology
ML	Maximum Likelihood
MMSE	Minimum Mean-Squared Error
MUSIC	Multiple Signal Classification
MVDR	Minimum Variance Distortionless Response
PHAT	Phase Transform
PLL	Phase-Locked Loop
QMF	Quadrature Mirror Filter
QPSK	Quadrature Phase-Shift Keying
RF	Radio Frequency
SINR	Signal-to-Interference-and-Noise Ratio
SNR	Signal-to-Noise Ratio
STAP	Space-Time Adaptive Processing
TDOA	Time Difference of Arrival
UAV	Unmanned Aerial Vehicle

This page intentionally left blank.

REFERENCES

[1] N. Vankayalapati, S. Kay, and Q. Ding, "TDOA based direct positioning maximum likelihood estimator and the Cramer-Rao bound," *IEEE Transactions on Aerospace and Electronic Systems* 50(3), 1616–1635 (2014).

[2] L.L. Scharf and B. Friedlander, "Matched subspace detectors," *Signal Processing, IEEE Transactions on* 42(8), 2146–2157 (1994).

[3] K.W. Forsythe, "Utilizing waveform features for adaptive beamforming and direction finding with narrowband signals," *The Lincoln Laboratory Journal* 10(2) (1997).

[4] K.W. Forsythe, D.W. Bliss, and C.M. Keller, "Multichannel adaptive beamforming and interference mitigation in multiuser CDMA systems," in *Conference Record of the Thirty-Third Asilomar Conference on Signals, Systems, and Computers (Cat. No. CH37020)*, IEEE (1999), vol. 1, pp. 506–510.

[5] A.J. Weiss, "Direct position determination of narrowband radio frequency transmitters," *IEEE Signal Processing Letters* 11(5), 513–516 (2004).

[6] J. Ward, "Space-time adaptive processing for airborne radar," MIT Lincoln Laboratory, Technical rep. (1994).

[7] L.A. Romero and J. Mason, "Evaluation of direct and iterative methods for overdetermined systems of TOA geolocation equations," *IEEE Transactions on Aerospace and Electronic Systems* 47(2), 1213–1229 (2011).

[8] S. Bancroft, "An algebraic solution of the GPS equations," *IEEE Transactions on Aerospace and Electronic Systems* (1), 56–59 (1985).

[9] J. Smith and J. Abel, "Closed-form least-squares source location estimation from range-difference measurements," 35(12), 1661–1669 (1987).

[10] K. Ho and W. Xu, "An accurate algebraic solution for moving source location using TDOA and FDOA measurements," *IEEE Transactions on Signal Processing* 52(9), 2453–2463 (2004).

[11] A.J. Weiss and A. Amar, "Direct geolocation of stationary wideband radio signal based on time delays and Doppler shifts," in *2009 IEEE/SP 15th Workshop on Statistical Signal Processing*, IEEE, pp. 101–104.

[12] J. Moon and L. Moser, "On the correlation function of random binary sequences," *SIAM Journal on Applied Mathematics* 16(2), 340–343 (1968).

[13] D.P. Young, C.M. Keller, D.W. Bliss, and K.W. Forsythe, "Ultra-wideband (UWB) transmitter location using time difference of arrival (TDOA) techniques," in *The Thrity-Seventh Asilomar Conference on Signals, Systems & Computers, 2003*, IEEE (2003), vol. 2, pp. 1225–1229.

[14] D.W. Bliss and A. Chan, "Synthetic aperture geolocation of cellular phones in the presence of multiple access interference," in *ASAP Proceedings* (2002).

[15] D.W. Bliss and K.W. Forsythe, "Angle of arrival estimation in the presence of multiple access interference for CDMA cellular phone systems," in *Proceedings of the 2000 IEEE Sensor Array and Multichannel Signal Processing Workshop. SAM 2000*, IEEE (2000), Cat. No. 00EX410, pp. 408–412.

[16] R. Tolimieri and S. Winograd, "Computing the ambiguity surface," *IEEE Transactions on Acoustics, Speech, and Signal Processing* 33(5), 1239–1245 (1985).

[17] G.C. Carter, "Coherence and time delay estimation," *Proceedings of the IEEE* 75(2), 236–255 (1987).

[18] K.W. Forsythe, L. Collins, and H. Naumer, "Beamforming with Distributed Arrays: FY19 RF Systems Line-Supported Program," MIT Lincoln Laboratory, Technical Rep. LSP-270 (Estimated publication date: December 2019).

[19] M. Zatman, "How narrow is narrowband?" *IEE Proceedings-Radar, Sonar and Navigation* 145(2), 85–91 (1998).

[20] I.S. Reed, J.D. Mallett, and L.E. Brennan, "Rapid convergence rate in adaptive arrays," *IEEE Transactions on Aerospace and Electronic Systems* (6), 853–863 (1974).

[21] D.G. Manolakis, V.K. Ingle, and S.M. Kogon, *Statistical and Adaptive Signal Processing*, Boston: McGraw-Hill (2000).

[22] I. Proudler and J. McWhirter, "QR decomposition based algorithms and architectures for lease-squares adaptive filtering," Royal Signals and Radar Establishment Malvern (United Kingdom), Technical rep. (1992).

[23] N. Kalouptsidis and S. Theodoridis, *Adaptive system identification and signal processing algorithms*, vol. 994, Prentice Hall New York (1993).

[24] D.R. Fuhrmann, "Application of Toeplitz covariance estimation to adaptive beamforming and detection," *IEEE Transactions on Signal Processing* 39(10), 2194–2198 (1991).

[25] T.Q. Nguyen, "Near-perfect-reconstruction pseudo-QMF banks," *IEEE Transactions on Signal Processing* 42(1), 65–76 (1994).

[26] W.A. Abu-Al-Saud and G.L. Stuber, "Efficient wideband channelizer for software radio systems using modulated PR filterbanks," *IEEE Transactions on Signal Processing* 52(10), 2807–2820 (2004).

[27] E.J. Kelly, "An adaptive detection algorithm," *IEEE Transactions On Aerospace And Electronic Systems* 22(1).

[28] R.O. Schmidt, "Multiple emitter location and signal parameter estimation," *IEEE Transactions on Antennas and Propagation* 34(3), 276–280 (1986).

[29] A.J. Weiss, "Direct geolocation of wideband emitters based on delay and Doppler," *IEEE Transactions on Signal Processing* 59(6), 2513–2521 (2011).